

Overexpression of the *Arabidopsis* Syntaxin PEP12/SYP21 Inhibits Transport from the Prevacuolar Compartment to the Lytic Vacuole in Vivo ^W

Ombretta Foresti, Luis L.P. daSilva, and Jürgen Denecke¹

Centre for Plant Sciences, Faculty of Biological Sciences, University of Leeds, Leeds LS2 9JT, United Kingdom

Golgi-mediated transport to the lytic vacuole involves passage through the prevacuolar compartment (PVC), but little is known about how vacuolar proteins exit the PVC. We show that this last step is inhibited by overexpression of *Arabidopsis thaliana* syntaxin PEP12/SYP21, causing an accumulation of soluble and membrane cargo and the plant vacuolar sorting receptor BP80 in the PVC. Anterograde transport proceeds normally from the endoplasmic reticulum to the Golgi and the PVC, although export from the PVC appears to be compromised, affecting both anterograde membrane flow to the vacuole and the recycling route of BP80 to the Golgi. However, Golgi-mediated transport of soluble and membrane cargo toward the plasma membrane is not affected, but a soluble BP80 ligand is partially mis-sorted to the culture medium. We also observe clustering of individual PVC bodies that move together and possibly fuse with each other, forming enlarged compartments. We conclude that PEP12/SYP21 overexpression specifically inhibits export from the PVC without affecting the Golgi complex or compromising the secretory branch of the endomembrane system. The results provide a functional in vivo assay that confirms PEP12/SYP21 involvement in vacuolar sorting and indicates that excess of this syntaxin in the PVC can be detrimental for further transport from this organelle.

INTRODUCTION

Protein targeting through the secretory pathway occurs through a complex sequence of transient protein–protein interactions, leading to conformational changes and further interactions controlling the next step in the pathway. These begin with the binding of cargo to specific receptors and the subsequent recruitment of protein coats that shape the donor membrane into a transport vesicle (Bonifacino and Glick, 2004). Soon after budding, the coat disassembles and recycles for a new round of vesicle budding. The naked vesicle then moves, possibly guided by the cytoskeleton, to the target compartment. The docking step is thought to be mediated by the Rab family of low molecular weight GTPases (Zerial and McBride, 2001) and a specific set of tethering factors that are capable of forming stable coiled-coil interactions (Pfeffer, 1999; Gillingham and Munro, 2003). Finally, vesicles fuse with the target membrane by interaction between soluble *N*-ethylmaleimide-sensitive fusion protein attachment protein receptors (SNAREs) (Chen and Scheller, 2001; Hong, 2005).

Due to their importance in the last step of vesicle docking and fusion, SNAREs are required for many of the membrane traffick-

ing events of the secretory pathway. They are generally tail-anchored membrane proteins characterized by a conserved 70–amino acid coiled-coiled domain (the SNARE motif) that precedes the C-terminal transmembrane domain. SNAREs reside either on the vesicle membrane (*v*-SNARE) or the target membrane (*t*-SNARE). According to the nature of their SNARE motifs, these proteins can also be classified into Q-SNAREs and R-SNAREs (Chen and Scheller, 2001; Fasshauer, 2003; Hong, 2005). Q-SNAREs are normally acting as *t*-SNAREs and are subdivided into the Qa, Qb, and Qc classes, whereas R-SNAREs are frequently *v*-SNAREs. The Qa class is also commonly referred to as syntaxin and is often the largest of the three Q-SNAREs. Prior to vesicle fusion, three Q-SNAREs on the target compartment interact with each other and with the R-SNARE on the transport vesicle (via their SNARE-motif) to form the typical four-helix SNARE complex that is thought to mediate membrane fusion (Jahn et al., 2003).

Due to the cyclic nature of membrane traffic in the secretory pathway, many machinery components are thought to recycle between compartments on a regular basis. This is particularly true for sorting receptors that recycle back to select new cargo and for the *v*-SNAREs that must return to the original donor membrane to be incorporated into new transport vesicles (Bonifacino and Glick, 2004). By contrast, *t*-SNAREs, in particular the syntaxins (Qa group), are enriched in the target membranes (Uemura et al., 2004). SNAREs must carry adequate sorting information to reach the correct destination and to accumulate to high steady state levels. However, small quantities of syntaxins will be present in transit through the endoplasmic reticulum (ER) and the Golgi apparatus since they are first inserted into the ER membrane (Borgese et al., 2003) and then exit this

¹ To whom correspondence should be addressed. E-mail j.denecke@leeds.ac.uk; fax 44-113-3433144.

The author responsible for distribution of materials integral to the findings presented in this article in accordance with the policy described in the Instructions for Authors (www.plantcell.org) is: Jürgen Denecke (j.denecke@leeds.ac.uk).

^WOnline version contains Web-only data.

www.plantcell.org/cgi/doi/10.1105/tpc.105.040279

organelle together with sorting receptors, cargo molecules, and other SNAREs.

How SNAREs in transit may be prevented from triggering undesired membrane fusion events was recently suggested by the identification of inhibitory SNARE activity (i-SNARE) (Varlamov et al., 2004). SNAREs could function in both fusogenic and nonfusogenic SNARE complexes, depending on their location, to avoid unspecific membrane fusion caused by SNARE machinery in transit. The authors suggested that nonfusogenic SNARE complexes (i-SNAREs) could have a physiological function at the level of the Golgi apparatus to increase the polarity of this organelle. This would ensure that ER-derived vesicles fuse with the *cis*-Golgi, while retrograde transport vesicles from endosomes fuse to the *trans*-Golgi, but it has yet to be shown if similar i-SNARE activity can be detected on other organelles. We are thus beginning to understand some of the multilayered biomolecular interactions that control membrane flow within the secretory pathway, but much is yet to be discovered.

Sorting of soluble hydrolases to the lytic vacuole in vegetative plant cells is thought to be dependent on the vacuolar sorting receptor BP80, as well as the *Arabidopsis thaliana* syntaxins PEP12/SYP21 and VAM3/SYP22, for Golgi-mediated delivery to the prevacuolar compartment (PVC) and ultimately the vacuole (Paris and Neuhaus, 2002; Jurgens, 2004). The two syntaxins were originally identified in a genetic screen for mutants with altered vacuolar morphology or that were defective in the delivery of the soluble vacuolar hydrolase carboxypeptidase Y (CPY) to the vacuole in *Saccharomyces cerevisiae* (Wada et al., 1992, 1997; Becherer et al., 1996; Darsow et al., 1997). In this organism, loss of pep12 function (Δ pep12) resulted in accumulation of 40- to 50-nm vesicles in the cytosol and enlargement of vacuoles. Biochemical analysis showed that at the nonpermissive temperature, CPY and other vacuolar hydrolases were no longer targeted from the *trans*-Golgi network to the PVC but were instead secreted into the medium in their Golgi-modified form (Becherer et al., 1996). Further work revealed that pep12p is required for fusion of *trans*-Golgi network-, early endosome-, and vacuole-derived membranes with the PVC (Gerrard et al., 2000a).

In *Arabidopsis*, At PEP12/SYP21 was isolated by complementation of the yeast Δ pep12 mutant, and it was shown to be expressed in all plant tissues (Bassham et al., 1995). Based upon sequence homology, it was classified in the SYP2 (for syntaxin of plants) group together with At VAM3/SYP22 (Sanderfoot et al., 2000; Pratelli et al., 2004). For simplicity, we will use the new terms SYP21 and SYP22 for the *Arabidopsis* homologs of yeast pep12 and vam3, respectively. Gene disruption of each member of the SYP2 class leads to lethal phenotypes in *Arabidopsis*, indicating that they serve essential nonredundant functions in vacuolar transport (Sanderfoot et al., 2001b).

SYP21 was shown to immunoprecipitate with the Qb-SNARE VTI11 and the Qc-SNARE SYP51 from plant extracts (Zheng et al., 1999; Sanderfoot et al., 2001a). It was also found on the PVC membranes where it colocalized with VTI11 and SYP51 (da Silva Conceicao et al., 1997; Sanderfoot et al., 1998, 2001a; Zheng et al., 1999; Bassham et al., 2000; Uemura et al., 2004). This corresponds well with the coprecipitation data and supports the view that these three SNAREs are likely to form a SNARE complex involved in Golgi-to-PVC trafficking (Zheng et al., 1999;

Sanderfoot et al., 2001a). SYP22 was both localized to the tonoplast and the PVC in *Arabidopsis* (Sato et al., 1997; Sanderfoot et al., 1999). A complex between SYP22, VTI11, and SYP51 has been suggested to operate at the tonoplast and may control PVC-to-vacuole traffic (Surpin et al., 2003; Yano et al., 2003).

It has recently been shown that the drug wortmannin inhibits the recycling of BP80 from the PVC, leading to increased leakage of receptors to the vacuole, followed by degradation (daSilva et al., 2005). The resulting receptor depletion at the Golgi apparatus manifests itself via the hypersecretion of soluble vacuolar proteins. It was postulated that the plant equivalent of the retromer-mediated pathway defined in *S. cerevisiae* (Seaman et al., 1997, 1998) would be wortmannin sensitive (Oliviusson et al., 2006). Although it appears to be clear that vacuolar sorting receptors, such as yeast VPS10 or the mammalian mannose-6-phosphate receptors, are rescued from the PVC to avoid degradation in the lytic environment of the vacuole (Seaman, 2005), it is not known how the last sorting step from the PVC to the vacuole takes place. In particular, it remains to be elucidated how soluble vacuolar proteins and tonoplast membrane proteins reach the vacuole while at the same time the receptor is rescued.

The steady state levels of BP80 or derived fluorescent fusion proteins are repeatedly found to be highest in the PVC, despite their recycling to the Golgi apparatus where they are thought to select cargo (Li et al., 2002; Tse et al., 2004; daSilva et al., 2005). Specific cargo transport from the PVC to the vacuole would require an additional vesicle transport step from the PVC to the vacuole that excludes entry of BP80. Alternatively, it could be proposed that PVCs fuse with the vacuole directly but only after active retrieval of sorting receptors and other components. The second model would thus postulate that PVCs must mature prior to fusion with the vacuole. Currently, there are no experimental data that can discriminate between these two models.

In this study, we have concentrated on the last step in the vacuolar transport pathway and show that overexpression of SYP21 provides an experimental tool to inhibit PVC-to-vacuole traffic in vivo. The sorting receptor and soluble and membrane-spanning proteins destined to the lytic vacuole are trapped in PVCs that appear to form clusters in the cells. Moreover, soluble vacuolar cargo is partially redirected to the cell surface. By contrast, the distribution and motility of Golgi bodies and constitutive traffic of soluble and membrane-spanning proteins to the plasma membrane remains unaffected. The possible mechanisms of syntaxin-mediated inhibition of membrane traffic are discussed.

RESULTS

Overexpression of the Syntaxin SYP21 Causes Secretion of Vacuolar Proteins without Affecting Constitutive Secretion

Dominant or semidominant effects of overexpressed molecules are often useful to gain insight into the function of gene products because they report on the consequences of protein actions. Previous studies on the tobacco (*Nicotiana tabacum*) plasma membrane SNARE Syr1 showed that overexpression of a truncated soluble fragment lacking its transmembrane domain (Sp2) inhibited secretion of a green fluorescent protein marker (sGFP). Under these conditions, GFP was effectively retained in the ER

and the Golgi apparatus, suggesting that interference with transport steps toward the plasma membrane has far-reaching consequences (Geelen et al., 2002). The effects of Sp2 on secretion could be suppressed by enhanced expression of wild-type SNARE Syr1. Sp2 probably interacts with one or several binding partners of Syr1, preventing them from forming a functional SNARE complex with endogenous Syr1, but this remains to be demonstrated.

We attempted a similar approach to interfere with the function of the syntaxin SYP21, previously reported to localize to the PVC together with the plant vacuolar sorting receptor BP80 (*Arabidopsis* ELP, BP80b, and VSR1) (Li et al., 2002; Tse et al., 2004). SYP21 includes a single membrane-spanning domain at its C terminus. We therefore placed either the full-length SYP21 coding region or the sequence covering the first 251 amino acids excluding the transmembrane domain under the transcriptional control of the cauliflower mosaic virus 35S (CaMV35S) promoter, generating the constructs SYP21 and SYP21 Δ TM, respectively (Figure 1A). SYP21 Δ TM is analogous to a soluble truncated form of the yeast pep12p (pep12STOP) that has previously been shown to complement the pep12 Δ phenotype when overexpressed (Gerrard et al., 2000b). It is likely that pep12STOP can still associate with the other partner of the SNARE complex despite lacking its transmembrane domain. It was therefore expected to act as competitor in our assay by analogy to the observation

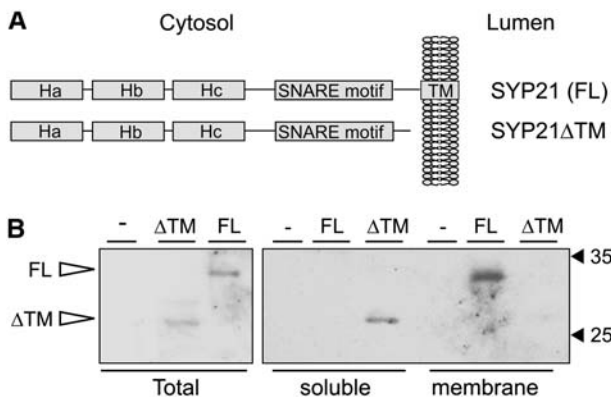


Figure 1. Expression of Recombinant Full-Length and Truncated SYP21.

(A) Schematic representation of the constructs used in this work. Either the full-length *Arabidopsis* SYP21 coding region or the sequence covering the first 251 amino acids comprising only the cytoplasmic domain was cloned under the transcriptional control of the CaMV35S promoter, generating the constructs full-length SYP21 and SYP21 Δ TM, respectively. Shown is the orientation in the membrane and the typical domain structure of Q_A-SNAREs consisting of the transmembrane domain, the SNARE domain, and the three α -helical repeats Ha, Hb, and Hc.

(B) Protoplasts were transfected with a constant amount (30 μ g) of plasmid encoding either full-length SYP21 (FL) or truncated SYP21 (Δ TM). After 24 h of incubation, cells were harvested. Protein extracts from entire protoplasts (total, left panel) and from soluble- or membrane-enriched fractions (right panel) were compared by protein gel blots and probed with anti-SYP21 antibodies. A mock-electroporated (–) sample was included to demonstrate the specificity of the antiserum. Molecular mass markers are indicated in kilodaltons.

made with the Sp2 fragment of tobacco Syr1 (Geelen et al., 2002).

To test the presence of the recombinant gene products, protoplasts were prepared from *N. tabacum* leaves and transfected with plasmid encoding either full-length SYP21 or truncated SYP21 Δ TM. Protein gel blots with α -SYP21 antibodies (Tse et al., 2004) show equal levels of expression of the two proteins in the total cell extract (Figure 1B, left panel). SYP21 showed an apparent molecular mass of 31 kD. The predicted SYP21 Δ TM is 28 amino acids shorter than the full-length molecule and on SDS-PAGE it migrated with higher mobility and an estimated molecular mass of 28 kD. The same cell populations were fractionated into soluble- and membrane-enriched fractions. As expected, SYP21 Δ TM was recovered exclusively in the soluble fraction, while the full-length SYP21 molecule was detected exclusively in the membrane fraction (Figure 1B, right panel).

To test the potential of the two recombinant genes to interfere with vacuolar sorting of soluble proteins, we used the model vacuolar cargo Amy-*spo*, an α -amylase fusion protein carrying the sequence specific sorting signal of sweet potato (*Ipomoea batatas*) sporamin. This fusion has been extensively tested and described previously as a BP80-dependent vacuolar transport cargo (Pimpl et al., 2003; daSilva et al., 2005). Protoplasts were transformed with a constant amount of plasmid encoding Amy-*spo*, together with increasing concentrations of plasmids encoding either SYP21 Δ TM (Figure 2A, Δ TM, gray bars) or full-length SYP21 (Figure 2A, FL, white bars). After 24 h, cells and incubation medium were separated, and the α -amylase activity was measured in both fractions. The ratio between the extracellular and intracellular enzyme activity was calculated and is shown as the secretion index, established to be a linear function of time at steady state (Phillipson et al., 2001; Pimpl et al., 2003). Full-length and truncated SYP21 were expressed at similar levels as illustrated by the protein gel blot below the graphs. Surprisingly, no effect was observed in the presence of SYP21 Δ TM at any concentration. By contrast, full-length SYP21 coexpression caused a substantially induced secretion of Amy-*spo* in a SYP21 dosage-dependent fashion.

To determine if the observed induction is specific for vacuolar targeting, we tested if the two constructs would affect the constitutive secretion of α -amylase (Amy). Figure 2B shows that neither gene product caused significant increases in Amy secretion. Although a minor upwards trend can be noted for the secretion index in response to increased SYP21 Δ TM dosage (Figure 2B, gray bars), the changes observed were within the range of the standard errors of these assays and thus not considered significant. Supplemental Figure 1A online illustrates this further by showing the individual activities for cells and medium.

The control experiment with the secretory cargo Amy was important because it ruled out a potential overall increase in secretory transport to the cell surface as a result of SYP21 overexpression. The very strong induction of Amy-*spo* secretion, resulting in a 35-fold increase in the secretion index, indicates that SYP21 overexpression specifically interferes with the vacuolar transport route and causes mistargeting to the cell surface.

Figure 3A shows that the increase in the secretion index of Amy-*spo* with full-length SYP21 overexpression (Figure 2A, white bars) was predominantly caused by an increase in the activity in

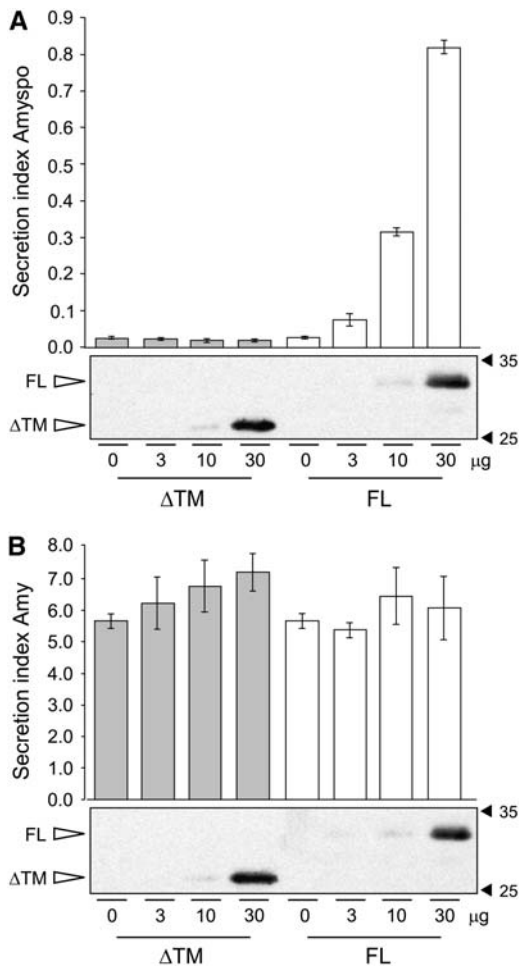


Figure 2. Effect of SYP21 Overproduction on Protein Transport to the Vacuole.

(A) Protoplasts were transfected with a constant amount of plasmid (10 μg) encoding the vacuolar cargo Amy-spo together with increasing concentrations of either SYP21ΔTM (ΔTM, gray bars) or full-length SYP21 (FL, white bars) encoding plasmids (amounts in micrograms are indicated below each lane). After 24 h of incubation, cells and medium were harvested and α-amylase activity was measured in each fraction. The secretion index was calculated as the ratio between the extracellular and the intracellular α-amylase activities. The mock-electroporated sample was used as blank for the α-amylase assays. Data are from five independent protoplast transfections ± SE. Total cell extracts were also loaded on SDS-PAGE for protein gel blotting to document the comparable expression of the two test effector molecules (FL and ΔTM). **(B)** Identical experiment to **(A)** except for the use of the secretory cargo Amy instead of the vacuolar cargo Amy-spo. All experimental conditions and annotations are as in **(A)**.

the medium (gray bars) while the activity in the cells (white bars) remains constant. The increase in the total activity is likely due to a higher stability of the enzyme in the culture medium compared with the lytic vacuole, which was observed before (Pimpl et al., 2003). The results also indicate that SYP21 overexpression compromises vacuolar transport in a different way compared with the drug wortmannin (Figure 3B). Indeed, in the presence of increas-

ing concentrations of the drug, Amy-spo was strongly redirected to the medium (gray bars), and its activity in the cells (white bars) was reduced drastically. In contrast with SYP21 overexpression, the drug reduces α-amylase synthesis (Pimpl et al., 2003) probably due to an adverse physiological effect. This difference prompted us to further investigate which step of the vacuolar transport is affected by SYP21 overexpression.

Overexpression of SYP21 Causes Intracellular Accumulation of Vacuolar Precursors

To gain further information on the transport step compromised by SYP21 overexpression, we used the vacuolar cargo GFP-spo. This molecule carries the same vacuolar sorting signal as Amy-spo but can be used for *in vivo* imaging and would enable us to see if and where intracellular accumulation of the protein occurs upon SYP21 overexpression. Moreover, it can also be analyzed by protein gel blotting, where it produces two characteristic degradation products, the presence of which indicates vacuolar sorting.

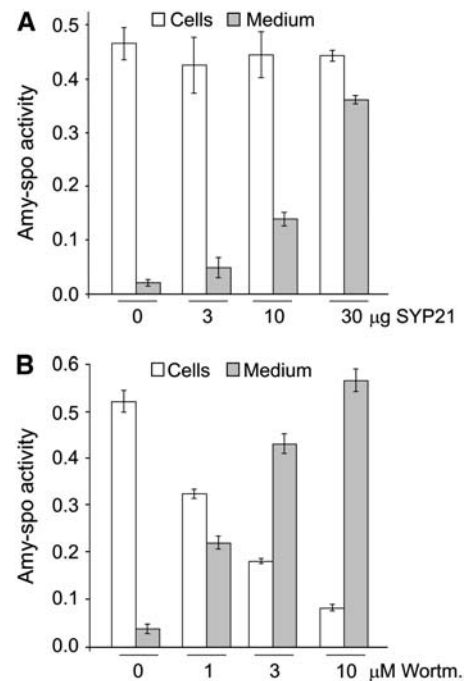


Figure 3. Comparison of the Effect of SYP21 Overexpression with That of the Drug Wortmannin.

(A) Individual cellular and extracellular α-amylase activities from experiments shown in Figure 2A (given in ΔOD per milliliter of protoplast suspension and per minute). Mock-electroporated sample was used as blank for all α-amylase assays. Data are from five independent protoplast transfections ± SE.

(B) Protoplasts were transfected with a constant amount (10 μg) of plasmid encoding the vacuolar cargo Amy-spo, distributed in equal portions, and then incubated with different concentrations of wortmannin (indicated in micromolar below each lane) for 24 h. Cells and media from five independent protoplast transfections were harvested, and α-amylase activity was measured in each fraction. All other annotations are as in **(A)**.

The first is a deglycosylated fragment that is formed in an as yet unidentified post-Golgi compartment en route to the vacuole, and the second is the lower molecular weight GFP-core fragment that can be purified from isolated vacuoles (daSilva et al., 2005). Both products can therefore be used to monitor the intracellular transport of GFP-spo.

Protoplasts were transformed with constant amounts of plasmid encoding GFP-spo and cotransfected with increasing amounts of SYP21-encoding plasmid. Cells and medium extracts were analyzed by protein gel blotting using anti-GFP antibodies. Figure 4A shows that an increasing concentration of SYP21 caused a reproducible reduction in the formation of the GFP-core and a partial redirection of the full-length glycosylated precursor to the medium. However, the most remarkable effect of the overexpression of SYP21 is the intracellular accumulation of the highest molecular weight glycosylated form of GFP-spo. This suggests a partial retention of the vacuolar cargo in a compartment with a lower proteolytic activity than the vacuole. Precursor accumulation at the expense of the GFP-core fragment leads to approximately equal cellular levels and corresponds

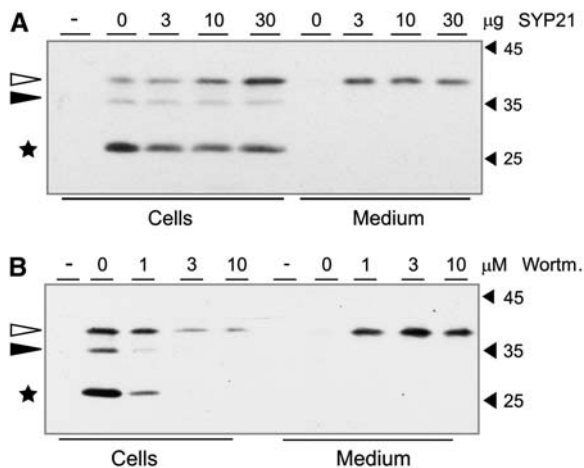


Figure 4. Effect of Wortmannin and SYP21 Overexpression on GFP-spo.

(A) A constant amount (10 µg) of GFP-spo was coexpressed with increasing concentrations of SYP21 encoding plasmid as effector. Cells and media were harvested, and equal quantities were analyzed by protein gel blotting and detection with anti-GFP antibodies. The effector plasmid concentration is given above each lane in micrograms. Glycosylated (white arrowheads) and unglycosylated (black arrowheads) precursors are clearly distinguished from the GFP core fragment (indicated by a star). Molecular mass markers are indicated in kilodaltons. Note the accumulation of the glycosylated precursor in the cell with an increasing concentration of SYP21.

(B) Protoplasts were transfected with a constant amount (10 µg) of plasmid encoding for GFP-spo, pooled and distributed in equal portions, followed by incubation in the presence of different concentrations of wortmannin for 24 h. Cells and media were harvested, and equal quantities were analyzed by protein gel blotting and detection with anti-GFP antibodies. The concentration of the drug is given above each lane. Annotations are as in **(A)**. Note that increasing concentrations of wortmannin reduce the formation of the unglycosylated precursor and the GFP core fragment and also decrease cellular levels of the glycosylated precursor.

well with the constant Amy-spo activity maintained in the cells under these conditions (Figure 3A). By contrast, with increasing concentrations of the drug wortmannin, the levels of both degradation intermediates are dramatically decreased, and the high molecular weight glycosylated precursor shows a significant drug dosage-dependent reduction of its cellular steady state levels (Figure 4B). The data are in agreement with the strong reduction in cellular Amy-spo activity that was observed as a consequence of wortmannin treatment (Figure 3B). The results with GFP-spo and Amy-spo illustrate a clear difference between the effect of SYP21 overexpression and that of the drug wortmannin on the traffic of soluble vacuolar cargo.

SYP21 Overexpression Traps Soluble Vacuolar Cargo in the PVC

We decided to investigate the intracellular localization of GFP-spo by confocal laser scanning microscopy (CLSM) analysis and to determine the effect of SYP21 overexpression. To simplify the identification of cells cotransfected with the vacuolar cargo and the effector, we designed a fluorescently tagged version of the SNARE. We therefore fused yellow fluorescent protein (YFP) at the N terminus of SYP21. Similar fluorescent chimeras of SYP21 have been previously shown to properly localize on the PVC in transient expression (Ueda et al., 2004; Uemura et al., 2004). More importantly, syntaxins have been shown repeatedly to tolerate N-terminal fusions without losing their biological activity, as documented by genetic complementation and further biochemical and cytological assays (Wooding and Pelham, 1998; Sanderfoot et al., 2001a; Niihama et al., 2005).

To expand these findings, we tested if the YFP fusion of SYP21 (YFP-SYP21) was still capable of inducing the secretion of Amy-spo when overexpressed, similar to our observations with the untagged wild-type molecule in Figures 2 to 4. We thus performed an experiment analogous to that in Figure 2, but using the YFP-tagged form of the full-length SYP21. Figure 5A shows that YFP-SYP21 increases the secretion index of Amy-spo in a similar manner as previously observed for the untagged version of the SNARE (Figure 2A), except that the effect is weaker. In addition, the overexpression of YFP-SYP21 does not affect the constitutive secretion of Amy (Figure 5B), confirming the specificity of the inhibition to the vacuolar route. Supplemental Figures 1B and 1C online show the breakdown into intracellular and extracellular activities. Furthermore, YFP-SYP21 was shown to be intact by detecting only the fusion protein of 62 kD (Figure 5, bottom panels). Comparable results were obtained with a GFP-tagged version of SYP21 (data not shown). Moreover, GFP- or YFP-tagged fusions of truncated SYP21 lacking its transmembrane domain failed to exhibit any measurable effect on the soluble cargo molecules Amy and Amy-spo and were confirmed to be soluble and cytosolic (data not shown).

We then tested the effect of the coexpression of high levels of the SNARE with the soluble cargo GFP-spo. Protoplasts expressing GFP-spo alone showed diffuse staining in the central vacuole as well as some staining in the ER at the periphery of the cell, representing proteins in transit through the secretory pathway (see Supplemental Figure 2 online, left panel). This is best appreciated in a cross section of the cell and is consistent with previous

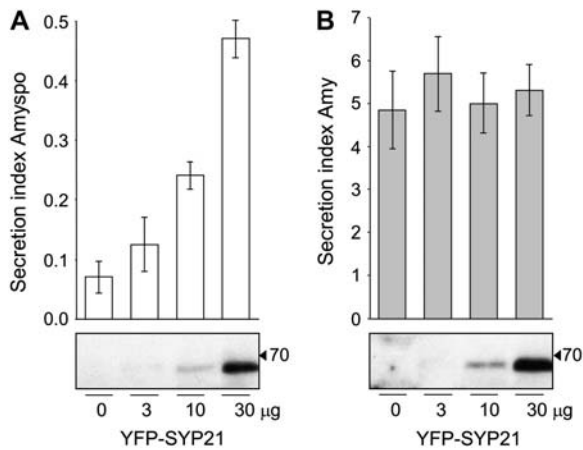


Figure 5. YFP-Tagged SYP21 Maintains Its Inhibitory Effect on Vacuolar Sorting.

Protoplasts were transfected with a constant amount of plasmid encoding either Amy-spo (**A**) or Amy (**B**) together with increasing concentrations of YFP-SYP21 plasmid preparation (as stated below each lane). After 24 h of incubation, cells and medium were harvested, and α -amylase activity was measured in each fraction. Data are from three independent protoplast transfections \pm SE. Membrane-enriched fractions were prepared from the same cell samples and analyzed by protein gel blotting using anti-GFP antibodies. Each lane corresponds to the α -amylase result above it. The molecular mass marker is indicated in kilodaltons. Note the comparable expression of the fusion protein in both panels.

reports (Sohn et al., 2003; daSilva et al., 2005) documenting vacuolar cargo in transit. At the level of the cell cortex (Figure 6A), the typical reticular pattern of the ER can be observed. This pattern did not change when low levels of the PVC marker YFP-BP80 were cotransfected (Figure 6A). This marker was shown to colocalize with endogenous BP80 (Tse et al., 2004) and does not affect vacuolar sorting when expressed at low levels (daSilva et al., 2005). GFP-spo only labeled the typical reticular pattern, and no specific enrichment of GFP-spo occurred in the highly defined punctate structures highlighted by YFP-BP80.

In the presence of overexpressed YFP-SYP21, the vacuolar cargo GFP-spo showed reduced delivery to the central lytic vacuole (see Supplemental Figure 2 online, right panel) as expected from the quantitative data from Figure 4A. More strikingly, at the cortex GFP-spo accumulated in well-defined punctate structures of variable size in addition to the amount of the vacuolar cargo in transit through the ER (Figure 6B). These discrete structures were mobile and clearly distinct from the ER network. They were colocalized with YFP-SYP21 (Figure 6B); therefore, they represent PVC compartments (da Silva Conceicao et al., 1997; Sanderfoot et al., 1998; Tse et al., 2004; Uemura et al., 2004). GFP-spo labeled the PVCs only when YFP-SYP21 was coexpressed (cf. Figure 6B with 6A). Similar punctate structures were observed when GFP-spo was cotransfected with untagged SYP21 (data not shown).

The accumulation of the GFP-spo cargo molecule in the PVC corresponds to the predicted accumulation in a less lytic compartment deduced from Figure 4A. It suggests that overexpres-

sion of SYP21 inhibits the last vacuolar transport step from the PVC to the vacuole, either by inhibiting PVC fusion with the central lytic vacuole or by interfering with an as yet uncharacterized vesicle-mediated route that operates between the PVC and the vacuole.

SYP21 Overexpression Traps a Tonoplast Protein in the PVC

To confirm the inhibition of membrane flow to the vacuole, we tested the effect of SYP21 overexpression on the intracellular transport of the YFP-fused vacuolar SNARE SYP22 (YFP-SYP22). This protein is well established as a tonoplast marker (Sato et al., 1997; Uemura et al., 2002, 2004) and would serve to test whether membrane traffic from the PVC to the vacuole is blocked under SYP21 overexpression. As expected from published findings, the majority of the protoplasts expressing YFP-SYP22 show clear tonoplast localization in the absence of SYP21 overexpression (Figure 6C). The presence of internal subregional structures, previously named bulbs, exhibiting a stronger fluorescence than the outer vacuolar membrane are also a typical feature of tonoplast staining (Mitsuhashi et al., 2000; Saito et al., 2002; Uemura et al., 2002).

In the presence of coexpressed GFP-SYP21, YFP-SYP22 accumulated in enlarged punctate structures that colocalized with the same compartment highlighted by GFP-SYP21 (Figure 6D). A block of transport from the PVCs to the central vacuole could explain that soluble and membrane cargo accumulates in the PVC, causing the formation of these enlarged structures. Interestingly, YFP-SYP22 did not mistarget to the plasma membrane, whereas the soluble cargo GFP-spo was significantly redirected to the cell surface (Figure 4A). It is yet unclear from which compartment the soluble cargo GFP-spo reaches the cell surface under these conditions.

Overexpression of SYP21 Does Not Prevent Membrane Flow from the Golgi Apparatus to the Plasma Membrane

Overexpression of SYP21 interferes with the targeting of soluble and membrane cargos to the vacuole (Figures 2 to 4). However, it does not interfere with the constitutive secretion of Amy (Figure 2B). This prompted us to investigate if SYP21 overexpression would affect the transport of a plasma membrane protein.

As shown before (Uemura et al., 2004), the syntaxin YFP-SYP121 strongly labels the plasma membrane when expressed in protoplasts, giving a characteristic ring pattern (see Supplemental Figure 3A online). This pattern remains unaltered upon coexpression with GFP-SYP21 (Figure 6E), suggesting that in contrast with YFP-SYP22, the transport of YFP-SYP121 was not inhibited. While the SYP21 fusion highlighted punctate and enlarged PVCs, the YFP-SYP121 fusion continued to reach the plasma membrane and was not trapped in GFP-SYP21-labeled structures. At the level of the cell cortex, it was observed that YFP-SYP121 labels punctate structures in addition to the predominant plasma membrane location (see Supplemental Figure 3B online), agreeing with previous observations (Uemura et al., 2004). Importantly, YFP-SYP121-labeled structures never contained signals from GFP-SYP21 and could either represent the plant equivalent of the early endosomes or the Golgi apparatus.

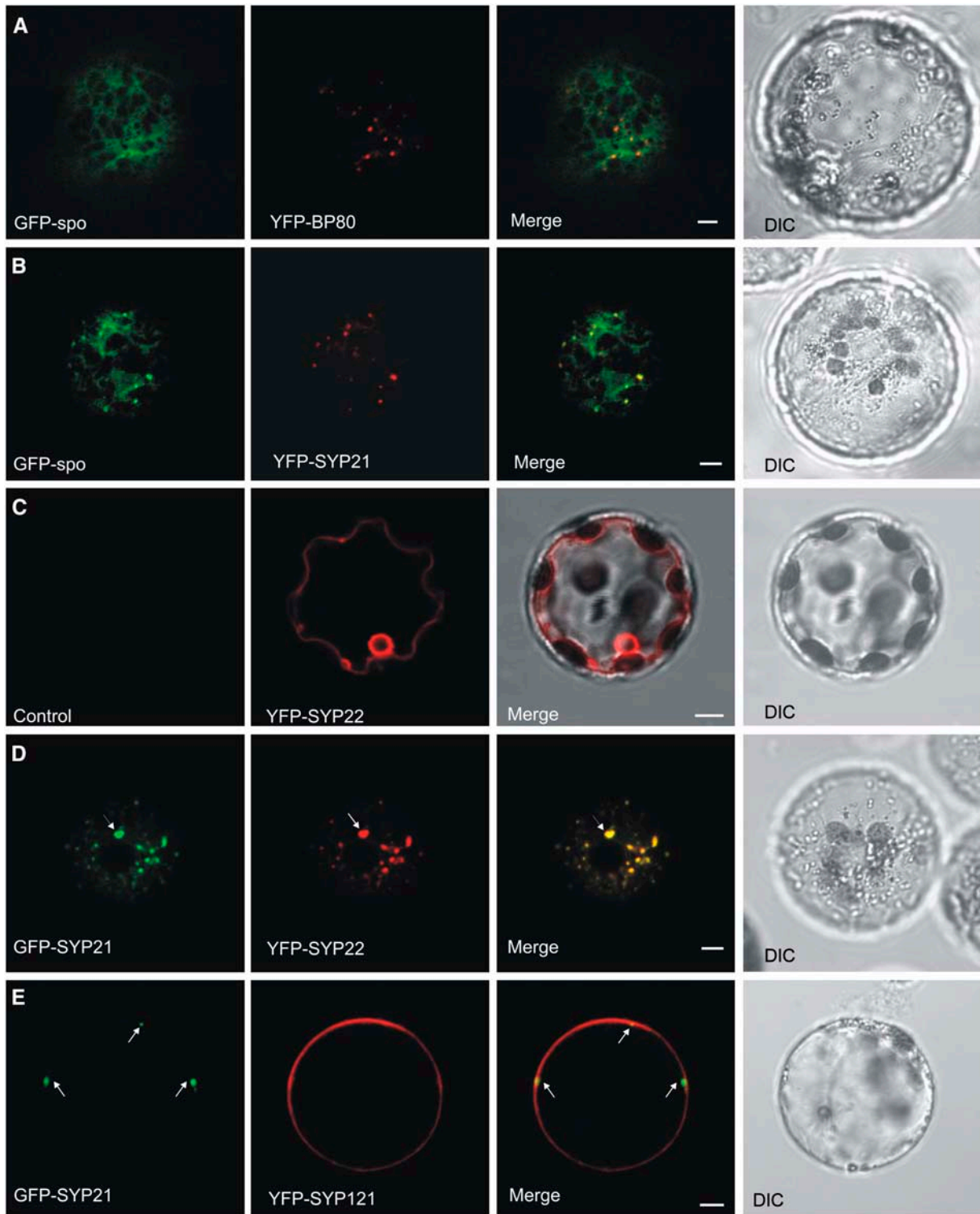


Figure 6. Specific Inhibition of Vacuolar Transport by SYP21 Overexpression.

(A) Transient expression experiment (16 h incubation) with tobacco leaf protoplasts electroporated with plasmids encoding the vacuolar cargo molecule GFP-spo and the PVC marker YFP-BP80. Shown is an image of the cell cortex excluding the vacuolar lumen from the pinhole to facilitate monitoring of the intermediate organelles of the secretory pathway (ER, Golgi, and PVC) contained within the cytosol. Signals from the two distinct fluorescent

Together, the data suggest that traffic to the plasma membrane occurs normally even with increased SYP21 expression, not only for soluble secreted proteins such as α -amylase (Figure 2B) but also for a membrane-spanning protein (Figure 6E).

SYP21 Overexpression Does Not Alter Golgi Morphology

Since the Golgi apparatus is the compartment at which the secretory and vacuolar transport routes divert, we tested if SYP21 overexpression would affect the morphology and distribution of this central compartment of the secretory pathway. Protoplasts were therefore prepared from a transgenic line stably expressing the Golgi marker ST-GFP and transfected with either the plasmid encoding YFP-BP80 or YFP-SYP21. Figure 7A shows cells transfected with YFP-BP80, displaying Golgi bodies (highlighted with ST-GFP) and PVCs (highlighted by YFP-BP80). Consistent with earlier studies documenting a partial localization of BP80 or YFP-BP80 in the Golgi apparatus (Tse et al., 2004; daSilva et al., 2006), it can be seen that many of the ST-GFP-labeled structures are also weakly stained by YFP-BP80 (Figure 7A, arrows). Cells transfected with YFP-SYP21 revealed no alterations in the structure and distribution of Golgi bodies (cf. Figures 7B and 7C with 7A). YFP-SYP21-highlighted structures were enlarged and remained clearly distinct from the ST-GFP-labeled Golgi bodies (Figures 7B and 7C). In contrast with YFP-BP80, YFP-SYP21 did not weakly stain the ST-GFP-labeled Golgi bodies, suggesting that progress of the SNARE to the PVC is very efficient.

Together with the normal progress of soluble and membrane-spanning proteins via the Golgi apparatus to the cell surface, the results suggest that SYP21 overexpression affects neither the transport of proteins from the ER to the Golgi apparatus nor the traffic from the Golgi apparatus to the PVC or plasma membrane. The block in protein traffic is thus very specific for the last step of vacuolar transport.

SYP21 Overexpression Induced Enlargement/Clustering of PVC Bodies

In the majority of the protoplasts, the structures labeled by YFP-SYP21, when expressed alone or in combination with ST-GFP, are fewer in number and bigger in dimension than the PVCs

highlighted by other markers, such as GFP/YFP-BP80 (cf. Figure 7A and data in da Silva et al., 2006 with Figures 7B and 7C). Statistical analysis of individual transfected protoplasts (Figure 7D) revealed that the number of individual YFP-BP80-labeled PVCs was slightly higher than ST-GFP-labeled Golgi bodies. By contrast, YFP-SYP21-labeled PVCs were threefold less frequent compared with Golgi numbers. The reduction in PVC numbers was accompanied by a noticeable shift in the frequency of large PVCs. While the majority of PVCs (92%) were smaller than 1 μ m in cells expressing YFP-BP80 as a marker, YFP-SYP21-expressing cells exhibited much higher numbers of PVCs between 1 and 2 μ m and above (Figure 7E). The clearest difference is seen with PVCs larger than 2 μ m, which were not observed without SYP21 overexpression.

The results suggest that SYP21 overexpression causes fusion or aggregation, which would explain both findings (Figures 7D and 7E). However, upon closer inspection of the enlarged PVC structures (Figures 7B and 7C), we noticed that the structures represent clusters of several smaller individual PVC bodies (Figures 7F and 7G). This was particularly clear in the time series of scanned images (Figures 7H to 7J; see Supplemental Movie 1 online). The clusters were highly variable in shape, but individual PVC bodies appeared to be tethered together during movement.

The results suggest that the observed enlargement of the PVCs may not actually be an increase in overall size but a result of stable associations of individual PVC bodies. This was investigated in more detail within the leaf epidermis (see below).

SYP21-Mediated Inhibition of Vacuolar Sorting Leads to Accumulation of GFP-BP80 in the PVC

To help understand how soluble cargo could be secreted by blocking export from the PVC, the next important question was to test the effect of SYP21 overexpression on the intracellular distribution of the vacuolar sorting receptor BP80. Unlike vacuolar cargo, BP80 is thought to recycle from the PVC back to the Golgi for further cargo selection and to avoid proteolysis in the lytic compartment (daSilva et al., 2005; Seaman, 2005). In the presence of the drug wortmannin, BP80 does not recycle and leaks to the vacuole, leading to receptor depletion in the Golgi apparatus and increased secretion of its ligands (daSilva et al.,

Figure 6. (continued).

molecules are shown individually (in green and red, respectively) or as a merge. Images in bright field (differential interference contrast [DIC]) are shown at the right. Note the reticular patterns for the vacuolar cargo that is in transit through the ER. Bar = 5 μ m.

(B) Similar experiment to **(A)** except that YFP-BP80 was replaced by YFP-SYP21. In contrast with **(A)**, GFP-spo was enriched in well-defined punctate structures well above the background level in the reticular structures and perfectly colocalized with the punctate signals by YFP-SYP21. Bar = 5 μ m.

(C) Transient expression experiment (24-h incubation) with tobacco leaf protoplasts electroporated with plasmids encoding the membrane-spanning protein YFP-SYP22. Shown is a cross section through a protoplast to allow visualization of the tonoplast. The control panel shows that no YFP signals bleed through to the GFP channel. The merge with DIC illustrates how the tonoplast meanders on the inside of the chloroplasts, which are found in between the tonoplast and the plasma membrane. Bar = 5 μ m.

(D) Transient expression experiment as in **(C)** except that GFP-SYP21 was cotransfected with YFP-SYP22. Notice that under these conditions, YFP-SYP22 is colocalized in punctate structures together with GFP-SYP21, some of which are particularly enlarged (arrows). Shown is a cortex view of the protoplast. Bar = 5 μ m.

(E) Transient expression experiment (24-h incubation) with tobacco leaf protoplasts transfected with plasmids encoding GFP-SYP21 and a YFP-tagged form of the plasma membrane syntaxin SYP121. Shown is a cross section of the protoplast to better visualize the plasma membrane. GFP-SYP21 overexpression does not influence the targeting of YFP-SYP121 to the plasma membrane. Bar = 5 μ m.

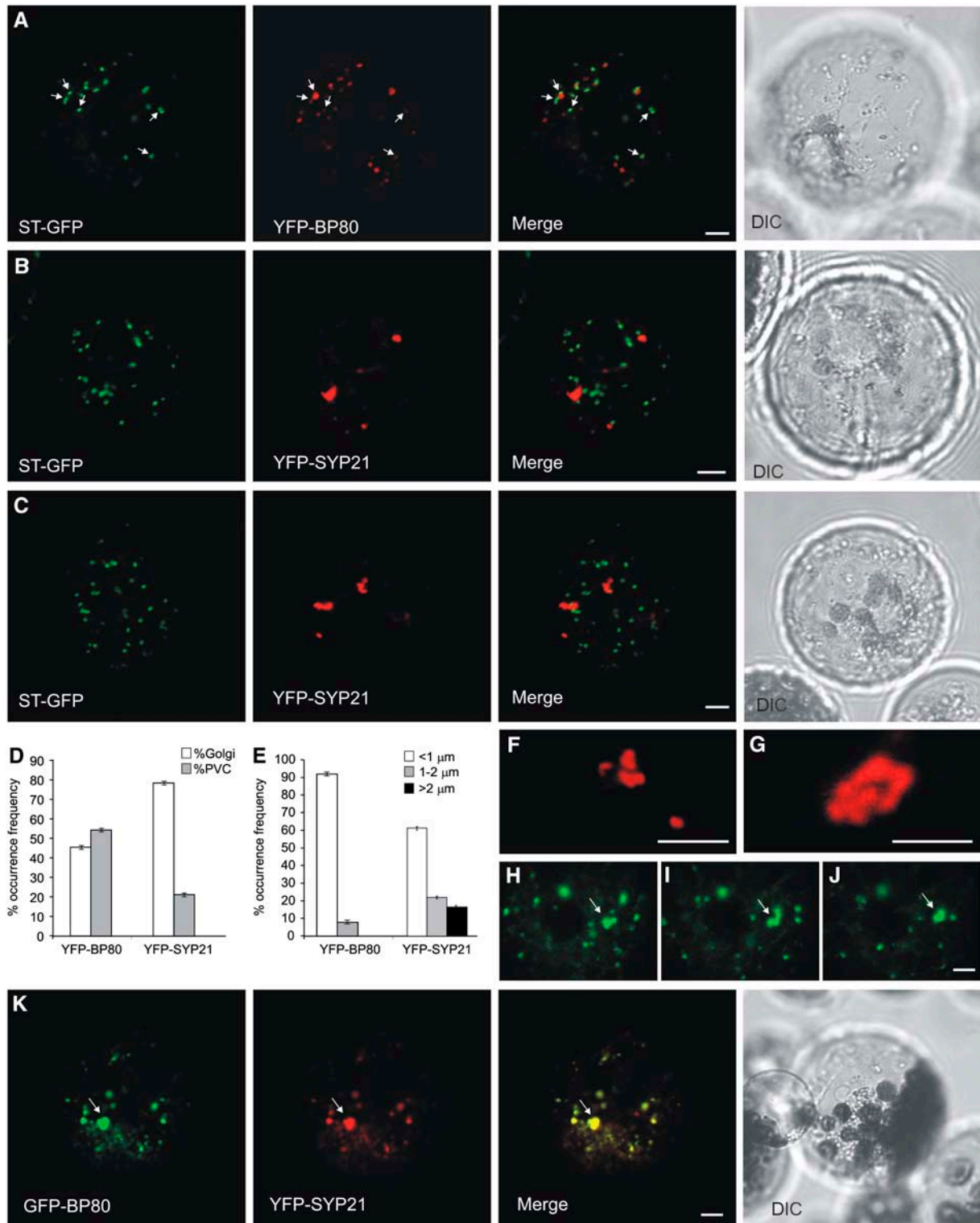


Figure 7. SYP21 Overproduction Perturbs PVC Morphology and Inhibits Recycling of the Plant Vacuolar Sorting Receptor.

(A) Transient expression experiment (16-h incubation) to document normal appearance of individual Golgi bodies highlighted with the marker ST-GFP (in green) and PVC bodies highlighted by YFP-BP80 (in red). Shown is a cortex view of the protoplast. Images in bright field (DIC) are shown at the right. Note that ST-GFP-labeled Golgi bodies are frequently weakly labeled by YFP-BP80 (arrows). Bar = 5 μm .

2005). Since SYP21 overexpression and wortmannin appear to affect cargo traffic in different ways, it was interesting to test the effect of increased SYP21 dosage on BP80 traffic.

We took advantage of the properties of the reporter protein GFP-BP80 to colocalize with the wild-type BP80 at the level of the Golgi apparatus and the PVC (Tse et al., 2004). Coexpression of GFP-BP80 with YFP-SYP21 revealed an almost perfect colocalization of the two markers (Figure 7K). However, in contrast with the typical small punctate distribution of GFP-BP80 (Figure 7A; daSilva et al., 2006), the marker also accumulated in enlarged PVCs (arrows) upon coexpression with YFP-SYP21, similar to the observation with YFP-SYP22 (Figure 6D). GFP-BP80 did not leak out to the vacuole as observed with the drug wortmannin (daSilva et al., 2005) but instead accumulated in the PVCs when SYP21 was overexpressed.

Statistical analysis of individual transfected protoplasts (Table 1) revealed that without SYP21 overexpression (i.e., Figure 7A), YFP-BP80 labels the PVC but also the Golgi apparatus (29% colocalization with ST-GFP), consistent with previous reports (Tse et al., 2004; daSilva et al., 2006). This is expected because YFP-BP80 is thought to recycle between these two compartments. In addition, the statistical analysis (Table 1) illustrates that almost none of the YFP-SYP21-labeled structures colocalize with the Golgi marker ST-GFP (1.5%; Figures 7B and 7C). When SYP21 is overexpressed (Figure 7K), we find an almost complete colocalization between SYP21 and coexpressed GFP-BP80 (96.5%) (Table 1). Should GFP-BP80 still recycle to the Golgi apparatus, a much lower degree of colocalization would be expected, allowing for 29% of the punctate GFP-BP80 signals to represent Golgi bodies and be distinct from PVC. This means that under SYP21 overexpression, the majority of YFP-BP80 has redistributed to the PVC.

These results suggest that the plant vacuolar sorting receptor neither leaves the PVC to return to the Golgi apparatus nor leaks out to the vacuole, but it is trapped together with its ligands in the PVCs. This could lead to a long-term depletion of receptors at the level of the Golgi apparatus, thus leading to partial secretion of the soluble ligands, such as Amy-spo (Figures 2 and 3) and GFP-spo (Figure 4A).

Table 1. Statistical Analysis of the Distribution of GFP-BP80 with Markers for the Golgi Apparatus and the PVC

	YFP-SYP21 versus ST-GFP	YFP-BP80 versus ST-GFP	YFP-SYP21 versus GFP-BP80
Percentage of colocalization	1.74	28.91	95.98
Error	0.15	1.35	0.16
Number of structures	805.00	762.00	616.00

The percentage of colocalization followed by the standard error and the total number of fluorescent punctate structures scored for three different types of cotransfections are shown. For each of the three cases, 15 individual images were scored.

Interference with PVC Export in Leaf Epidermis Cells by SYP21 Overexpression

All the experiments presented so far have been performed in tobacco leaf protoplasts. To test if similar observations could be made within intact tissues, we took advantage of the *Agrobacterium tumefaciens* infiltration method (Neuhaus and Boevink, 2001) that allows stable integration of transgenes into leaf epidermis cells. This method has been used extensively to visualize the morphology of secretory pathway organelles, such as the ER or the Golgi apparatus.

Figure 8A shows a cortical view of a portion of a transgenic tobacco leaf epidermis cell expressing the Golgi marker ST-GFP and YFP-SYP21. The latter was produced transiently as a result of infiltration with *A. tumefaciens*. The result shows that the coexpression of YFP-SYP21 did not alter the distribution of the Golgi marker, confirming the data obtained with protoplasts (Figures 7B and 7C). YFP-SYP21 did not colocalize with ST-GFP, and YFP-SYP21-labeled structures were present in low numbers and formed enlarged clusters. At high magnification (Figures 8B to 8E), it could also be appreciated that clusters are formed of circular shapes tethered together, reaching overall dimensions in excess of 5 μm . As observed in protoplasts, these large grape-like structures retained mobility, as documented in Supplemental

Figure 7. (continued).

(B) and **(C)** Overexpression of YFP-SYP21 (16-h incubation) does not influence the morphology of Golgi bodies in the cells while PVCs form large clusters. Note that ST-GFP-labeled Golgi bodies are not labeled by YFP-SYP21 and that there is no bleeding through of YFP signals in the GFP channel. Bars = 5 μm .

(D) Statistical analysis of the occurrence frequency of Golgi bodies (white bars) and PVC bodies (gray bars). The frequency is shown in percentage of the total number of punctate signals in a sample, and data are from 15 independent samples \pm SE in each case, scoring 762 individual punctate structures for YFP-BP80/ST-GFP and 805 for YFP-SYP21/ST-GFP. Note a clear shift to lower PVC numbers relative to Golgi numbers when YFP-SYP21 is used as PVC marker.

(E) Statistical analysis of the occurrence frequency for PVC bodies highlighted by either YFP-BP80 or YFP-SYP21 that are smaller than 1 μm (white bars), between 1 and 2 μm (gray bars), and above 2 μm (black bar). The frequency is shown as a percentage of the total number of punctate signals in a sample, and data are from nine independent samples \pm SE (386 punctate structures scored in total) for YFP-BP80 and 30 independent samples (262 punctate structures scored in total) for YFP-SYP21. Note a clear shift to large PVCs when YFP-SYP21 is overexpressed.

(F) and **(G)** Two examples of PVC clusters highlighted by YFP-SYP21, shown at high magnification. Notice that SYP21 overexpression causes the formation of clusters that appear to be composed of distinct PVC bodies tethered together. Bars = 5 μm .

(H) to **(J)** Still images of Supplemental Movie 1 online, showing the first, middle, and last frames. Note the variable shape of the PVC clusters highlighted by the arrows. Bar = 5 μm .

(K) Transient expression experiment showing subcellular localization of cotransfected YFP-SYP21 and GFP-BP80. Notice the almost complete colocalization of the two PVC markers and the enlarged structures (arrows). Bar = 5 μm .

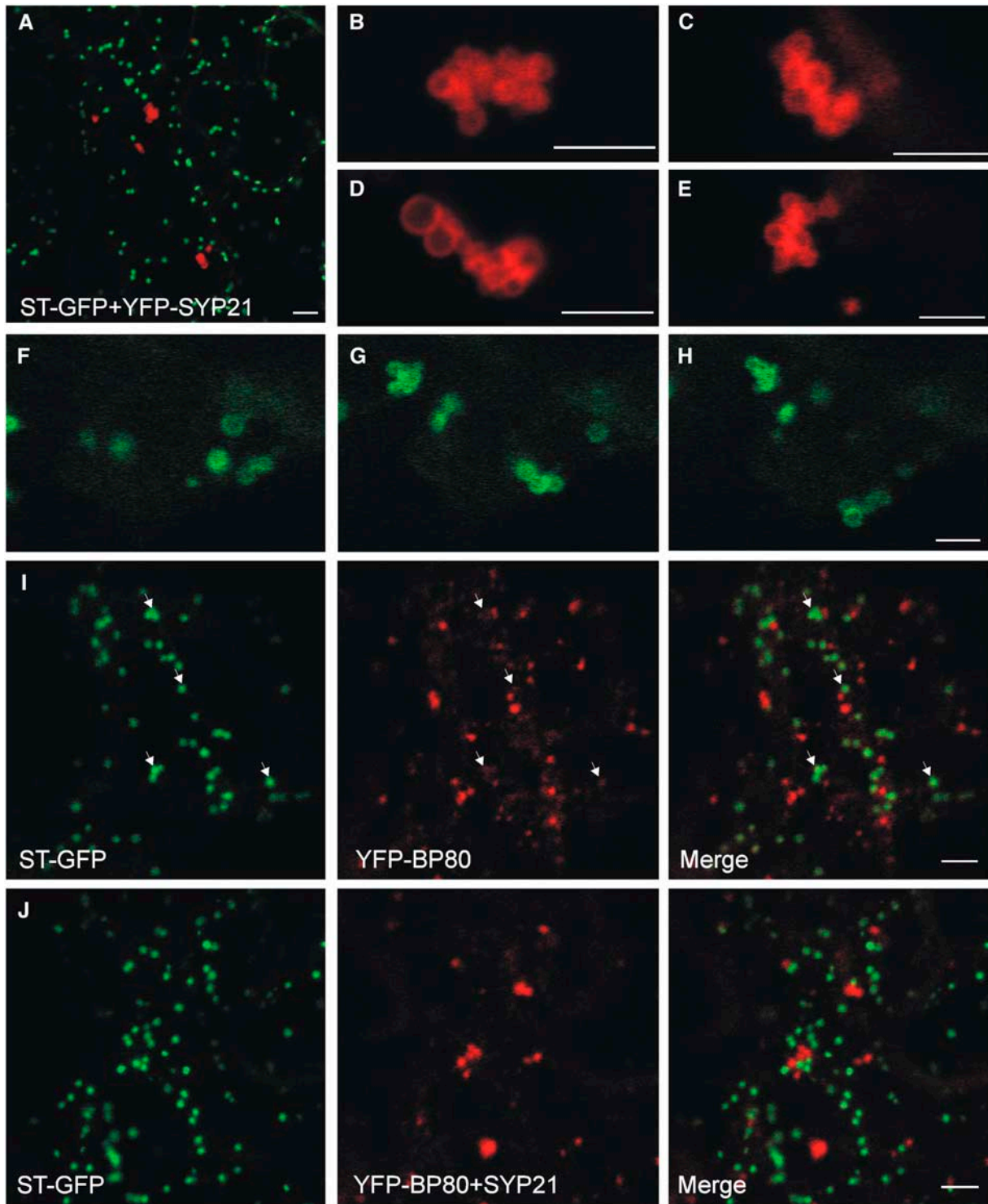


Figure 8. SYP21 Overexpression Causes PVC Clustering in Leaf Epidermis Cells.

(A) *Agrobacterium* infiltration experiment (2-d incubation) to document normal appearance of individual Golgi bodies highlighted with the Golgi marker ST-GFP (in green) and clustered PVC bodies highlighted by YFP-SYP21 (in red). Shown is a cortex view of a tobacco leaf epidermis cell. Bar = 5 μ m.

(B) to (E) Four examples of PVC clusters highlighted by YFP-SYP21, shown at high magnification. Notice that SYP21 overexpression causes the formation of clusters that appear to be composed of distinct PVC bodies. Bars = 5 μ m.

(F) to (H) Still images of Supplemental Movie 2 online, showing the first, middle, and last frames. Bar = 5 μ m.

Movie 2 online (Figures 8F to 8H). In addition, such enlarged clusters were not observed without SYP21 overexpression.

To rule out that SYP21-induced PVC clustering is due to fluorescent tagging, we transiently expressed YFP-BP80 in epidermis cells of the transgenic ST-GFP line, either with or without untagged wild-type SYP21. Figure 8I shows that YFP-BP80 expression alone gave rise to small punctate PVC labeling. It can also be seen that ST-GFP-stained structures are also weakly labeled with YFP-BP80, consistent with its recycling between the PVC and the Golgi apparatus (arrows). When SYP21 was coexpressed, a sharp decline in the numbers of YFP-BP80-labeled structures was observed as well as enlargement. Together, the results show that the clustering is not due to fluorescent tagging of SYP21 and confirm the data obtained from the protoplast system (Figures 6D and 6E). Moreover, ST-GFP-labeled structures were no longer stained by YFP-BP80, suggesting that recycling to the Golgi apparatus is compromised.

SYP21 Overexpression Traps Vacuolar Membrane Proteins in the PVC

Both SYP21 and SYP22 form complexes with VTI11 and SYP51, although the two complexes are thought to be formed on distinct compartments and mediate different transport steps (Zheng et al., 1999; Sanderfoot et al., 2001a; Surpin et al., 2003; Yano et al., 2003). Therefore, it could not be ruled out that the effect of trapping SYP22 in the PVC by SYP21 overexpression (Figure 6D) was restricted to this class of SNARE. For this reason, we wanted to test if the transport of another abundant tonoplast protein would be impaired by SYP21 overexpression.

Transgenic plants expressing a fluorescently tagged tonoplast aquaporin (BobTIP26-1-GFP) (Reisen et al., 2005) were infiltrated with *A. tumefaciens* strains to transiently express YFP-SYP22 alone or together with untagged wild-type SYP21. Figure 9A shows that BobTIP26-1-GFP and YFP-SYP22 colocalized at the level of the tonoplast. As expected, expression of YFP-SYP22 alone did not give rise to aberrant phenotypes. When SYP21 was coexpressed, most of the YFP-SYP22 was retained in bright punctate structures, while very little reaches the tonoplast (Figure 9B). Since YFP-SYP22 was expressed at the same time as the effector SYP21, a large proportion of this syntaxin was retained at the PVC. By contrast, BobTIP26-1-GFP was present at steady state levels prior to transient expression of SYP21, and only the de novo synthesized portion accumulated in punctate structures together with YFP-SYP22 (Figure 9B, arrows). A similar partial retention of BobTIP26-1-GFP can be observed when YFP-SYP21 was overexpressed (Figure 9C, arrows).

The results suggest that SYP21-mediated retention of membrane-spanning proteins is not restricted to SYP22 but also occurs when other tonoplast proteins are studied as cargo mol-

ecules. In addition, the results illustrate that despite the strong similarity between SYP21 and SYP22, only SYP21 overexpression causes PVC clustering and blocks export from this compartment.

DISCUSSION

Overexpression of Full-Length SYP21 Disrupts Protein Targeting

In *Arabidopsis*, the PVC syntaxin SYP21 is essential for cell development. This was demonstrated through gene disruption, which was lethal to the male gametophyte (Sanderfoot et al., 2001b). Because the lethality of this mutant occurs at an early stage of development, it was not possible to determine with this approach for which cellular function this protein is essential (Sanderfoot et al., 2001b). As an alternative approach, in this study, we transiently overexpressed SYP21 in plant cells to gain insight into the function of the encoded gene product.

It was previously reported that the overexpression of a truncated soluble version (Sp2 fragment) of a tobacco plasma membrane syntaxin (Syr1) inhibited transport toward the target compartment (Geelen et al., 2002), confirming the role of this SNARE in this transport step. By analogy, we constructed the corresponding soluble fragment of SYP21 (SYP21 Δ TM) and tested the effect of its overexpression on the transport of vacuolar cargo. In our system, SYP21 Δ TM did not affect protein targeting, while overexpression of the full-length wild-type SYP21 inhibited transport of soluble and membrane cargo to the vacuole and caused a partial redirection of soluble but not membrane cargo to the cell surface. SYP21 overexpression specifically interfered with vacuolar targeting without affecting constitutive secretion, suggesting that ER export and Golgi-to-plasma membrane transport occurred normally.

In the case of the tobacco plasma membrane syntaxin Syr1, the opposite was observed: the full-length molecule did not inhibit but restored correct targeting (Geelen et al., 2002). This discrepancy between the two types of SNAREs may reflect differences in the mechanism of vesicle targeting to an intermediate compartment (such as the PVC) and the plasma membrane. It is unlikely that the differences are due to the nature of the model systems because we verified the effect of SYP21 overexpression in leaf epidermis cells and found the same accumulation of vacuolar cargo in enlarged PVC clusters (Figures 9B and 9C). It cannot be completely ruled out that an *Arabidopsis* syntaxin may not function properly in tobacco, but the fact that it complements the Δ pep12 mutant in the yeast *S. cerevisiae* (Bassham et al., 1995) suggests a high conservation across kingdoms.

We therefore favor the first explanation that also corresponds well with similar observations made for another t-SNARE residing

Figure 8. (continued).

(I) *A. tumefaciens* infiltration experiment (2-d incubation) to document normal appearance of individual Golgi bodies highlighted with the Golgi marker ST-GFP and PVC bodies highlighted by YFP-BP80. Shown is a cortex view. Examples of Golgi bodies weakly labeled by YFP-BP80 are highlighted by arrows. Bar = 5 μ m.

(J) Overexpression of YFP-SYP21 does not influence the morphology of Golgi bodies in the cells while PVCs form large clusters. Notice the lack of colocalization between ST-GFP and YFP-BP80. Bar = 5 μ m.

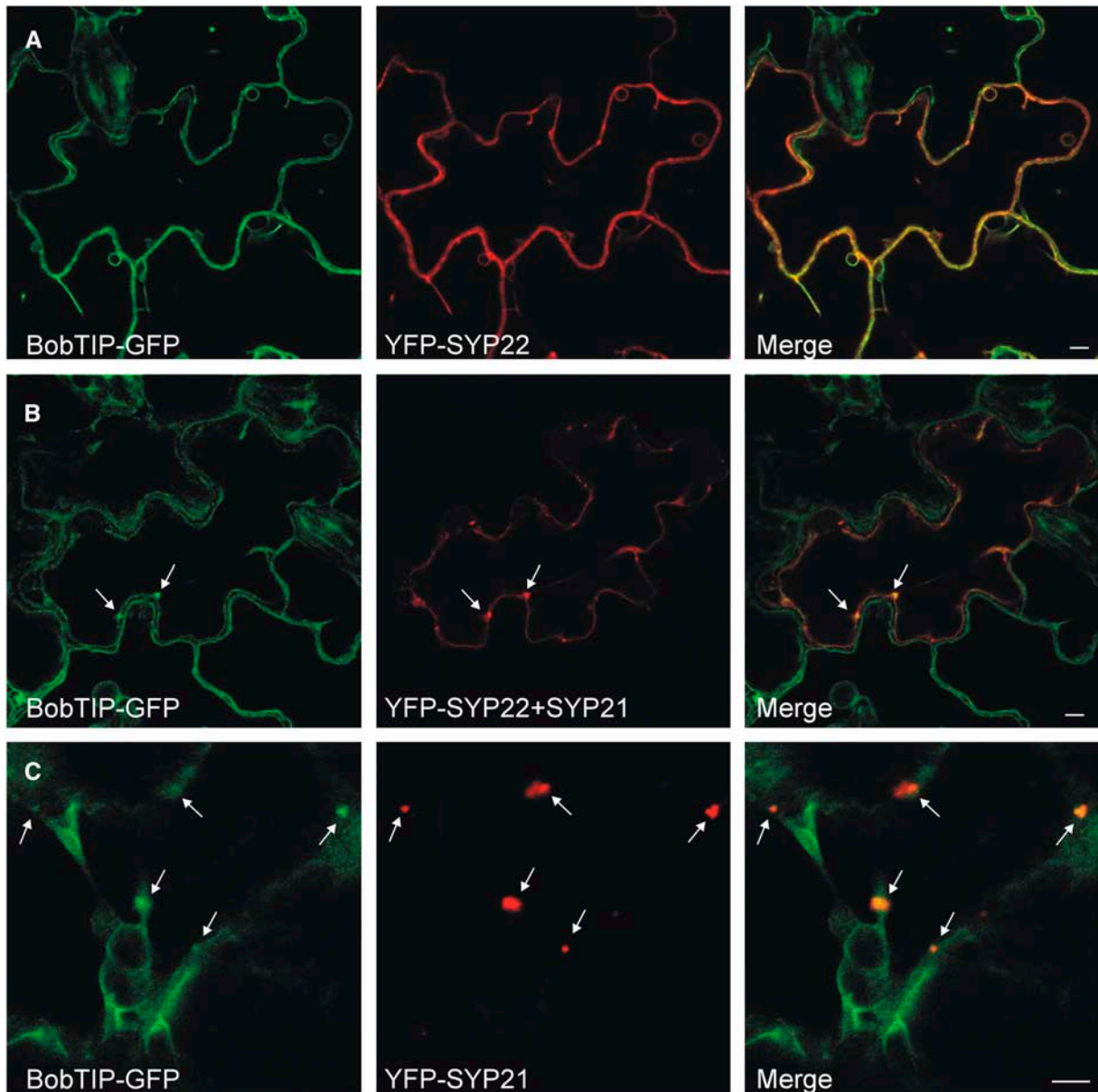


Figure 9. SYP21 Overproduction Perturbs Vacuolar Targeting of a Tonoplast Aquaporin.

(A) *A. tumefaciens* infiltration experiment using a transgenic tobacco line expressing BobTIP26-1-GFP as tonoplast marker and coexpressing YFP-SYP22. Notice the colocalization of the two tonoplast proteins. Bar = 5 μ m.

(B) As in **(A)** but transient YFP-SYP22 expression was supplemented with transient SYP21 overexpression. Notice that most of the YFP-SYP22 is localized in punctate structures, together with a portion of the BobTIP26-1-GFP (arrows). Bar = 5 μ m.

(C) As in **(A)** but with transient YFP-SYP21 expression. Note the punctate structures in which BobTIP26-1-GFP and YFP-SYP21 colocalize (arrows). Bar = 5 μ m.

on internal membranes, the Golgi syntaxin Sed5. This protein was identified as a multicopy suppressor of an ERD2 mutant (Hardwick et al., 1992) and found to cause a general reduction in anterograde ER-to-Golgi traffic, thus compensating for the ERD2 defect. Similar inhibitory effects were observed for the overexpressed full-length Golgi SNAREs Bos1 and Sec22 in tobacco epidermis cells (Chatre et al., 2005).

SYP21 Overexpression Traps Vacuolar Proteins in the PVC

Although both wortmannin treatment and SYP21 overexpression cause redirection of soluble vacuolar cargo to the medium, they appear to interfere with vacuolar transport in a distinct manner. Wortmannin treatment caused a redirection of the vacuolar marker Amy-spo to the culture medium at the expense of intracellular levels (Figure 3B). By contrast, SYP21 overexpression led to an

increase in the total Amy-spo activity, inducing the secretion of Amy-spo but maintaining intracellular levels. It is likely that the inhibition of vacuolar sorting prevented turnover of Amy-spo in the vacuole, as suggested before (Pimpl et al., 2003).

SYP21 overexpression also led to intracellular accumulation of the GFP-spo precursor and a simultaneous decrease of the vacuolar GFP core fragment (Figure 4A), while under wortmannin treatment, both precursor and degradation products decreased in response to increasing concentrations of the drug (Figure 4B). Therefore, the drug caused an overall decrease in the intracellular levels of GFP-spo, whereas SYP21 overexpression led to a qualitative shift from the vacuolar-processed fragment to the precursor, suggesting retention in an intracellular compartment prior to the vacuole.

Microscopy analysis confirmed that GFP-spo accumulates in punctate structures that colocalized with YFP-SYP21-labeled compartments (Figure 6B). This accumulation was not observed when another PVC marker (YFP-BP80) was coexpressed with GFP-spo (Figure 6A). This suggests that in addition to this induced secretion, SYP21 overexpression traps a portion of the soluble vacuolar cargo in the PVC. Similarly, the tonoplast markers YFP-SYP22 (Figures 6D and 9B) and BobTIP26-1-GFP (Figures 9B and 9C) were retained in the PVC when SYP21 was overexpressed. Together, these observations indicate that the main effect of SYP21 overexpression is a block of transport between the PVC and the vacuole.

Gene knockouts of SYP21 are lethal in *Arabidopsis* (Sanderfoot et al., 2001b), but the effects of pep12p disruption are well documented in yeasts (Becherer et al., 1996; Gerrard et al., 2000a). In contrast with our observations with overexpressed SYP21, its absence causes a defect of vesicle traffic toward the PVC either from the Golgi apparatus, the early endosomes, or the vacuole. It would be interesting to test pep12p overexpression in the yeast system and monitor the effect on the traffic of the yeast vacuolar sorting receptor VPS10, the vacuole syntaxin Vam3p, and soluble vacuolar cargo, such as CPY.

Interestingly, a similar block of PVC export was observed by interfering with the activity of the PVC-localized Rab5 homolog Rha1 (Sohn et al., 2003). Expression of the dominant-negative GDP-locked mutant Rha1[S24N] inhibited vacuolar transport of soluble cargo, causing their partial redirection to the medium and accumulation in PVCs. Rabs are thought to recruit tethering factors to initiate vesicle fusion with target organelles or organelle fusion itself (Zerial and McBride, 2001). It would be interesting to test the effects of the Rab mutant on the targeting of tonoplast proteins, but the striking similarity in the effects of SYP21 overexpression and Rha1[S24N] coexpression on the soluble cargo may indicate a functional link between Rab5 and SYP21 activity.

SYP21 Overexpression Causes Partial Secretion of Vacuolar Proteins

While SYP21 overexpression caused an accumulation of soluble and membrane vacuolar cargos in the PVCs, the morphology of the Golgi apparatus and the transport of soluble and membrane proteins to the cell surface were not affected (Figures 2B and 6E). This suggests that ER-to-Golgi traffic and the routes from the Golgi toward the plasma membrane or the PVC are not depen-

dent on SYP21 and that only the last step from the PVC to the vacuole is compromised by SYP21 overexpression. The partial secretion of the soluble cargo (Amy-spo and GFP-spo) was in contrast with that of a tonoplast protein, which was trapped in the PVC but did not reach the plasma membrane.

The observed secretion of vacuolar cargo in the presence of SYP21 overexpression (Figures 2 to 4) could be caused by their redirection to the cell surface from the Golgi apparatus or directly from the PVC. The latter pathway has been reported in *S. cerevisiae* (Harsay and Schekman, 2002), where it is believed to operate in addition to the default route from the Golgi, but there is no direct evidence for a similar route in plants so far. If this pathway is present and GFP-spo follows this route to the plasma membrane, we would also expect to observe a partial redirection of membrane vacuolar cargo to the cell surface. However, this was not observed for YFP-SYP22 (Figure 6D).

We also observed an accumulation of the reporter GFP/YFP-BP80 in the PVCs when coexpressed with SYP21 (Figures 7K and 8J). This reporter was shown to colocalize with the wild-type BP80 at the level of PVCs (Tse et al., 2004) and simulates endogenous BP80 traffic (daSilva et al., 2005). It also colocalizes weakly with the Golgi marker (Figures 7A and 8I, Table 1), consistent with its proposed recycling between the PVC and the Golgi (Tse et al., 2004; daSilva et al., 2006). When SYP21 was overexpressed, this colocalization with the Golgi marker was almost undetectable (cf. Figure 8I with 8J, Table 1). Instead, GFP-BP80 was almost exclusively colocalized with YFP-SYP21 (Figure 7K, Table 1), and no overlap between the Golgi marker ST-GFP and YFP-SYP21 was observed (Figures 7B, 7C, and 8A, Table 1). Furthermore, no mistargeting of GFP-BP80 was observed to the plasma membrane upon SYP21 overexpression (Figure 7E).

Together, these results suggest that both SYP21 and BP80 can efficiently reach the PVC from the Golgi apparatus. In addition, although the results are indirect, they strongly suggest that the plant vacuolar sorting receptor is trapped in the PVC when SYP21 is overexpressed. It does not leak to the vacuole, as reported for the effect of wortmannin (daSilva et al., 2005), but it is probably not able to recycle efficiently back to the Golgi apparatus, hence the reduced colocalization with the Golgi marker. As a consequence of defective recycling, BP80 levels would drop in the Golgi apparatus, as they would only be replenished from de novo synthesized molecules. With limiting receptors at the level of the Golgi apparatus, cargo molecules would be partially secreted by default. This would explain why some of the soluble cargo is secreted and some still reaches the PVC where it accumulates together with the sorting receptor. For these reasons, we favor the model in which BP80 ligands are mis-sorted from the Golgi apparatus, rather than from the PVC.

Enlargement/Clustering of PVC Bodies Induced by SYP21 Overexpression

In the majority of protoplasts expressing SYP21, PVCs appear to be enlarged well beyond 1 μm and consist of clusters of smaller PVC bodies (Figures 7D, 7E, 8B, and 8E). These clusters were found to undergo continuous reshaping and remodeling (Figures 7H to 7J and 8F to 8H; see Supplemental Movies 1 and 2 online)

and were present when GFP/YFP-SYP21 was expressed alone or together with other soluble or membrane markers (Figures 7 to 9). They were also observed when the untagged SYP21 was co-expressed with the PVC marker YFP-BP80 (Figure 8J), ruling out the possibility that clusters were artifacts caused by the YFP/GFP fusion. Both the clustering and the effects on cargo and receptor were observed with untagged and tagged SYP21 constructs (cf. Figures 2 and 5). This corresponds well with previous observations where N-terminal tagging of syntaxins did not compromise their activity (Wooding and Pelham, 1998; Sanderfoot et al., 2001a; Niihama et al., 2005).

It would be interesting to further characterize these clusters ultrastructurally and conduct proteomics analysis to determine if they have an altered physiology. If all the soluble and membrane proteins are trapped in them, they might gradually acidify and acquire higher proteolytic activity than normal PVCs, possibly resembling small vacuoles. This would explain why SYP21 overproduction only results in a modest reduction of GFP core formation but a significant increase in glycosylated precursor (Figure 4A).

How Can Overexpression of a Syntaxin Cause a Block in PVC Export?

SYP21 resides at the PVC and is supposed to be required for targeting to this intermediate organelle in the vacuolar transport route (Gerrard et al., 2000a). Other SNAREs, Rabs, and tethering and regulatory factors are required (Pfeffer, 1999; Sanderfoot and Raikhel, 1999; Nebenfuhr, 2002), but the interactions between them are still largely uncharacterized. At the level of the PVC, SYP21 is expected to interact with three other SNAREs to generate a functioning SNARE complex. Binding studies suggest that it interacts with the Qb-SNARE VTI11 (Zheng et al., 1999; Bassham et al., 2000) and the Qc-SNARE SYP51 (Sanderfoot et al., 2001a). The R-SNARE involved in the same SNARE complex is currently unknown, but likely candidates are the synaptobrevin homologs At VAMP-711/712/713 because they are found on PVCs and the tonoplast (Uemura et al., 2004).

Each functional SNARE complex requires three Q-SNAREs and one R-SNARE to generate a fusogenic complex (Jahn et al., 2003). After vesicle fusion with the target compartment, the SNARE complex needs to dissociate again. This event is mediated by regulatory factors like NSF (for *N*-ethylmaleimide-sensitive factor) and α -SNAP (for soluble NSF attachment protein) that require ATP to dissociate the complex (Bassham and Raikhel, 1999). The overexpression of a syntaxin might cause the production of partial unproductive SNARE complexes interacting with only one or two of the partners, leading to titration. Another possibility is that the recycling event is limiting and the fusogenic complex does not dissociate.

VTI11 and SYP51 have been reported to interact with SYP22 and presumably form a SNARE complex (Surpin et al., 2003; Yano et al., 2003) independently of SYP21. This has been suggested because SYP21 and SYP22 do not directly interact with each other (Sanderfoot et al., 2001a). The SYP22 complex might mediate the last transport step between the PVC and the vacuole. VTI11 and SYP51 could be titrated by SYP21, either because they are engaged in partial unproductive SNARE com-

plexes or because they cannot dissociate. As a consequence, the PVC might not be able to fuse with the vacuole or vesicles might not be able to bud from the PVC for subsequent fusion with the tonoplast. This will have the effect of trapping soluble components and membranes at the level of PVCs and causing their enlargement/clustering. Likewise, if the SNARE complex does not dissociate, the v-SNARE would not be able to recycle to the original donor membrane. This could explain why GFP-BP80 is also trapped in the PVC and appears to recycle less to the Golgi apparatus (Figures 7K and 8J, Table 1).

The recent identification of inhibitory SNAREs (i-SNAREs) may shed light on some of the dilemmas in the functioning of SNARE complexes (Varlamov et al., 2004). It was shown that both v-SNAREs and t-SNAREs can act as i-SNAREs and create nonfusogenic complexes when they are present in excess or accumulate in the wrong membrane. It was suggested that such i-SNARE activities could increase the polarity of the Golgi apparatus and create a secondary level of control, suitable to deal with stress-mediated or developmental fluctuations in the membrane flow. These studies suggested that the ratio of individual SNAREs is closely regulated in the different membranes of the secretory pathway and that imbalances can be detrimental.

Our results suggest that SYP21 overexpression results in a block of transport from the PVC to either the vacuole or the Golgi apparatus. This does not appear to be a general feature of syntaxins, and it is interesting to note that overexpression of the closely related SYP22 does not exhibit such a phenotype (Figure 9A; O. Foresti, unpublished results). Unraveling the differences between SYP21 and SYP22 will be an interesting challenge for the future. It will also be possible to test if specific SNAREs are titrated by reconstitution experiments using a combination of the assays used in this study. This should contribute to our understanding of the last sorting step in the vacuolar pathway, the separation of the sorting receptor from the cargo, and the delivery of the latter to the lytic vacuole.

METHODS

Recombinant Plasmid Production

All DNA manipulations were done according to established procedures. The highly competent *Escherichia coli* MC1061 strain (Casadaban and Cohen, 1980) was used for the routine amplification of all plasmids. Previously established plasmids were used, encoding α -amylase (Crofts et al., 1999), Amy-HDEL (Phillipson et al., 2001), Amy-spo (Pimpl et al., 2003), GFP-BP80, and GFP-SPO (daSilva et al., 2005).

The full-length coding region of SYP21 was amplified using sense oligo 5'-GACTAGCATCGATGAGTTTCAAGATTTAGAATCA-3' and antisense oligo 5'-TTGATGTCTAGACCAAGACAACGATGATGAC-3' from first-strand cDNA prepared as described previously (Pimpl et al., 2003), except that 5-d-old *Arabidopsis thaliana* seedlings were used for RNA extraction. The underlined regions refer to engineered restriction sites for insertion in pLL4 (Brandizzi et al., 2003) between the CaMV35S promoter at the *Cla*I site overlapping with the start codon and the *Xba*I site overlapping with the stop codon preceding the 3'-untranslated end of the nopaline synthase gene (3' nos). This created the chimeric expression plasmid pOF19 to produce untagged natural wild-type SYP21 in plant cells. Construction of the truncated fragment lacking the C-terminal transmembrane domain (SYP21 Δ TM) was performed in the same way, except for the use of the

antisense oligo 5'-AGTCGGTCTAGATTAAGTTTTAGCTGCTTTTCTG-3', thus yielding plasmid pOF31 to produce SYP21ΔTM in plant cells.

To engineer SYP21 and SYP21ΔTM fusions to the GFP, an *EcoRI*-*BglII* fragment carrying the CaMV35S promoter followed by the GFP coding region was cut out of the cytosolic GFP expression plasmid cGFP described previously (Brandizzi et al., 2003) and ligated together with an annealed *BglII*-*Clal* linker into either plasmid pOF19 for fusion to SYP21 or pOF31 for fusion to SYP21ΔTM. The linker was created by annealing the sense (5'-GATCTCAGCAGGTGGAGCAT-3') and antisense (5'-CGATGCTCCACCTGCTGA-3') oligos, yielding a fragment encoding the symmetric linker peptide SerAlaGlyGlyAlaSer for optimal positioning and functional maintenance of the SYP21 function within the context of a GFP fusion. pOF19 and pOF31 were cut with *EcoRI* and *Clal*, followed by dephosphorylation and subsequent ligation to both fragments. This yielded pOF22 expressing GFP-SYP21 and pOF34 expressing GFP-SYP21ΔTM.

To engineer a SYP21 fusion to the YFP, we amplified the YFP coding region using sense oligo 5'-GACTAGCCATGGTGAGCAAGGGCGAGG-AGC-3' and antisense oligo 5'-GAAACTCATCGATGCTCCACCCTTGTA-CAGCTCGCCATGCC-3'. Underlined regions refer to engineered restriction sites for subcloning as an *NcoI*-*Clal* fragment. The antisense oligo introduces a tetrapeptide (GlyGlyAlaSer) between the natural C-terminal Lys codon of YFP and the N-terminal Met codon of the SYP21 coding region. After cutting with *NcoI* and *Clal*, the obtained fragment was ligated together with the above-described *Clal*-*XbaI* SYP21 fragment into the expression plasmid pAmy-HDEL (Phillipson et al., 2001). The latter was cut with *NcoI* and *XbaI*, followed by dephosphorylation, for insertion of both fragments between the CaMV35S promoter and 3' nos, yielding pOF21 to express YFP-SYP21.

To generate the YFP-SYP22 fusion, the full-length coding region of SYP22 was amplified using sense oligo 5'-GACTAGCATCGATGAGTTT-TCAAGATTAGAATCA-3' and antisense oligo 5'-TCGAAATCTAGATTA-AGCTGCGAGTACTATAATCAC-3' from first-strand cDNA from 5-d-old *Arabidopsis* seedlings as described above. The underlined regions refer to engineered restriction sites *Clal* overlapping with the N-terminal Met codon and *XbaI* just following the stop codon of the SYP22 coding region. The obtained PCR fragment was digested with *Clal* and *XbaI*, gel purified, and ligated into pOF21 that was cut with *Clal* and *XbaI*, followed by dephosphorylation, to replace the SYP21 coding region by that of SYP22. This yielded plasmid pOF25 (YFP-SYP22).

To generate YFP-SYP121 fusion, a similar strategy was used as for SYP21, using the sense (5'-TCAGCCATCGATGATCCATATGAT-GTTCTGATTATTCTTGAATCCCGCGGGATCAACC-3') and antisense (5'-TTCAACTGGATCCTCAACTCAGCCTTGC-3') oligos for amplification from cDNA. The fragment was inserted as a *Clal*-*BamHI* fragment into pOF21 that was cut with *Clal* and *BamHI*, followed by dephosphorylation, to replace the SYP21 coding region by that of SYP121. This yielded plasmid pOF44 (YFP-SYP121).

To generate a YFP-BP80 fusion, we took advantage of the fact that differences in the amino acid sequence between GFP and YFP are restricted to the region 3' of the unique *NcoI* site present in GFP. We thus amplified this portion of YFP using the sense oligo 5'-CTGCCCGTG-CCATGGCCACCCTCGTGACCACC-3' and the antisense oligo 5'-ACA-AATCAGATCTCGGATCCTTCTGCTCCCTGTACAGCTCGTCCA-3'. The PCR fragment was digested with *NcoI* and *BglII* to yield a fragment that can replace the equivalent portion in pLL38, previously described as a GFP-BP80 expression plasmid (daSilva et al., 2005). This yielded plasmid pLL50 encoding YFP-BP80 that carries a signal peptide of sweet potato (*Ipomoea batatas*) sporamin for insertion into the ER.

Plant Material and Transient Protoplast Expression Procedure

Plants, *Nicotiana tabacum* cv Petit Havana (Maliga et al., 1973) or stable transgenic tobacco producing the Golgi marker ST-GFP (a kind gift of

Chris Hawes, Oxford, UK), were grown from surface-sterilized seeds in Murashige and Skoog medium (Murashige and Skoog, 1962) and 2% sucrose in a controlled room at 22°C with a 16-h daylength at the light irradiance of 200 μE m² s. Preparation of tobacco leaf protoplasts was done using 1× digestion mix, prepared from TEX buffer (B5 salts, 500 mg/L MES, 750 mg/L CaCl₂ [2 H₂O] 250 mg/L NH₄NO₃, and 0.4 M sucrose [13.7%], brought to pH 5.7 with KOH) supplemented with 0.2% Macerozyme R10 and 0.4% Cellulase R10 (Yakult). Stocks with 10-fold concentrated enzymes were prepared by dissolving the lyophilized powders in TEX buffer for 2 h, followed by centrifugation at 5000g for 15 min and filter sterilization (0.2 μm) of the clear supernatant. Aliquots (5 mL) of filtered supernatant were kept at -80°C for routine use. The 1× digestion mix was always prepared freshly by adding 45 mL of TEX buffer to these stocks. Overnight digestions of floating leaves, previously perforated using a needle bed (Phillipson et al., 2001), were followed by filtering through 100-μm nylon mesh and brief washing of the cell debris with electroporation buffer (0.4 M sucrose [13.7%], 2.4 g/L HEPES, 6 g/L KCl, and 600 mg/L CaCl₂, brought to pH 7.2 with KOH) to release further protoplasts from the tissue remnants. The protoplast suspensions were then centrifuged in Falcon tubes (50 mL) for 15 min at 100g at room temperature in a swing-out rotor. Centrifugation was stopped without brake to prevent resuspension of the floating protoplast band. The pellet and the underlying medium were removed and discarded using a peristaltic pump and a sterile Pasteur pipette until the band of floating living protoplasts reached the bottom. After resuspending the cells in 25 mL of electroporation buffer and a further centrifugation at 100g for 10 min, the pellet and the underlying medium were removed again. This procedure was repeated twice. After the final wash, protoplasts were resuspended in electroporation buffer at a concentration of 5 × 10⁶ protoplasts/mL. A total of 500 μL of the obtained protoplasts mix was pipetted into a disposable 1-mL plastic cuvette and mixed with an appropriate amount of plasmid DNA or mixtures of plasmids previously dissolved in 100 μL of electroporation buffer. The protoplast suspensions were then incubated for 5 min, followed by electroporation with stainless steel electrodes at a distance of 3.5 mm, using a complete exponential discharge of a 1000-μF capacitor charged at 160 V. After 15 min of absolute rest, electroporated protoplasts were removed from the cuvettes by washing in 1 mL of TEX buffer twice and transferred to 5-cm Petri dishes. Plasmid concentrations used are given in the figure legends. All incubations were performed for 24 h unless otherwise indicated.

Harvesting of cells and medium from 2.5 mL of cell suspension was initiated by 5 min of centrifugation. Approximately 1 mL of the underlying medium was manually removed with a refined Pasteur pipette. The medium was further cleared by centrifugation in a refrigerated microfuge (4°C, 18,000g, 10 min), and the obtained supernatant was kept on ice for further analysis (see below). To recover the total cell population of the remaining suspension, the cells were diluted 10-fold with 250 mM NaCl in 15-mL Falcon tubes. This washing step allows recovery of a compact cell pellet after 3 min of centrifugation at 200g. The resulting supernatant was removed with a peristaltic pump, and the pellets were kept on ice for subsequent extraction and analysis (see below).

α-Amylase Assay and Calculation of Secretion Index

Harvested cells and cleared culture medium from protoplast suspensions were processed to allow quantitative α-amylase detection. Medium was twofold diluted in α-amylase extraction buffer (50 mM acid malic, 50 mM sodium chloride, 2 μM calcium chloride, 0.02% w/v sodium azide). Cell pellets were resuspended in α-amylase extraction buffer to obtain a final volume of precisely 500 μL (including the volume of the resuspended cells). Soluble proteins were extracted by sonication for 5 s (amplitude 10 μm), followed by centrifugation for 10 min at 18,000g at 4°C and recovery of the supernatant.

The α -amylase assays were done routinely using the Megazyme substrate (R-CAAR4) consisting of blocked P-nitrophenyl maltoheptaoside (BPNPG7, 54.5 mg) and thermostable α -glucosidase (125 units at pH 6.0), dissolved according to the manufacturer's instructions in 10 mL of distilled autoclaved water and stocked at -80°C as 1-mL aliquots. Assays were started by adding 30 μL of substrate to 30 μL of sample, followed by incubation at 42°C , and the reaction was stopped by addition of 150 μL of 1% (w/v) Trizma base. A precise volume of 200 μL of each reaction was transferred into wells of a microtitre plate, and the absorbance was read at $\lambda = 405$ nm. Negative controls for correction of absorbance were obtained using medium and cell extracts from mock-transformed protoplasts.

The α -amylase activity was calculated in terms of change in optical density (ΔOD), divided per milliliter of extract used (taking into account the twofold dilution of the medium and the fivefold concentration of the cell extract relative to the original 2.5-mL suspension), and divided by the length of the assay in minutes. Only readings within the linear range between ΔOD 0.1 and 1.0 were used for calculations to avoid inaccuracy or substrate limitations. Once appropriate dilutions and incubation times were established, the assay was repeated at least three times for each extract, and the average activity was calculated. In all figures, such experiments were repeated at least three or up to five times using independent protoplast transfections, including all the controls.

The secretion index in each protoplast suspension was calculated as the ratio between the extracellular and the intracellular activity and thus represents digits without units. The error bars were calculated as the standard error from at least three or up to five independent protoplast transfections, as indicated in the legends.

Tobacco Leaf Infiltration Procedure

Soil-grown *N. tabacum* cv Petit Havana (Maliga et al., 1973) or transgenic plants producing BobTIP26-1-GFP (Reisen et al., 2005) were infiltrated with *Agrobacterium tumefaciens* cultures (at OD 0.1) as described previously (Neuhaus and Boevink, 2001) and analyzed after 2 d of further growth by CLSM.

Drug Incubations

Wortmannin was dissolved as a 33 mM stock solution in DMSO and subsequently diluted in TEX buffer as appropriate. The final concentration and incubation time in the presence of the drug are as described in the results and in the figure legends. To ensure constant background parameters for drug dosage experiments, a slightly modified electroporation protocol was used. The 600- μL batches of electroporated protoplast suspensions (containing 2.5×10^6 cells and plasmid DNA) were initially diluted with 1000 μL of TEX medium and then pooled. The protoplasts were then split into equal portions of 1000 μL and supplemented with another 1000 μL of TEX medium, which contains twice the final concentration of the drug indicated in the figure legends. This ensured minimal variation between the samples except for the concentration of the drug. Individual samples were then harvested as described above. Calculation of the secretion index was performed as described above except for using volumetric calculations based on a total cell suspension volume of 2 mL instead of 2.5 mL.

Protein Extraction and Gel Blot Analysis

Protein analysis of culture medium was performed after concentration with aqueous ammonium sulfate solution (60% final) for 2 h on ice, using BSA at 0.5 mg/mL as a carrier. From 600 μL of culture medium, proteins were precipitated by 10 min of centrifugation at 4°C in a refrigerated Eppendorf centrifuge at maximum speed, then resuspended in 60 μL of α -amylase extraction buffer to obtain a 10-fold higher concentration com-

pared with the original volume of cell suspension. The cell pellet obtained from 2.5 mL was resuspended in 250 μL of α -amylase extraction buffer (Phillipson et al., 2001), and soluble cell proteins were extracted by sonication and centrifugation for 10 min at $25,000g$ at 4°C . The supernatant containing the soluble proteins was recovered. Protein gel blots and immunodetection were performed as described by Pimpl et al. (2006) except for the use of rabbit polyclonal antiserum raised against GFP (1:5000 dilution; Molecular Probes) and α -SYP21 (1:1000 dilution; Tse et al., 2004).

CLSM

Infiltrated tobacco leaf squares (0.5×0.5 cm) were mounted in tap water with the lower epidermis facing the cover glass (22×50 mm; No. 0). Protoplasts expressing the GFP/YFP and fusions were harvested 24 h after transformation and by washing in TEX medium and concentration to a density of $\sim 2 \times 10^6/\text{mL}$ to obtain sufficient cell densities to identify transfected protoplasts. Protoplast suspension (100 μL) was pipetted into a 0.5×1 -cm rectangular cutout of a 150- μm -thick electrical tape covering a standard glass slide that offered a gap for hosting the cells. After covering the droplets with the cover glass ($22 \text{ mm} \times 50 \text{ mm}$; No. 0), slides were inverted and confocal imaging was performed using an inverted Zeiss LSM 510 META laser scanning microscope (Zeiss) with a Plan-Neofluar $\times 40/1.3$ oil DIC objective. For imaging of the coexpression of YFP and GFP constructs, excitation lines of an argon ion laser of 458 nm for GFP and 514 nm for YFP were used alternately with line switching on the multitrack facility of the microscope. Fluorescence was detected using a 545-nm dichroic beam splitter and a 475- to 525-nm band-pass filter for GFP and a 560- to 615-nm band-pass filter for YFP. Post-acquisition image processing was performed with the LSM 5 image browser (Zeiss).

Accession Numbers

Sequence data from this article can be found in the GenBank/EMBL data libraries under accession numbers L41651 (PEP12/SYP21), U88045 (VAM3/SYP22), and NM_202559 (SYP121).

Supplemental Data

The following materials are available in the online version of this article.

Supplemental Figure 1. Separate Intracellular and Extracellular Activities from Figures 2B, 5A, and 5B.

Supplemental Figure 2. YFP-SYP21 Overproduction Reduces Vacuolar Transport of GFP-spo.

Supplemental Figure 3. GFP-SYP21 Overproduction Does Not Influence Plasma Membrane Targeting of YFP-SYP121.

Supplemental Movie 1. YFP-SYP21 Labels Small Highly Mobile PVCs and Large PVC Clusters in Transfected Tobacco Leaf Protoplasts.

Supplemental Movie 2. YFP-SYP21 Labels Small Highly Mobile PVCs and Large PVC Clusters in Tobacco Leaf Epidermis Cells.

ACKNOWLEDGMENTS

This work was supported by grants from the Biotechnology and Biological Sciences Research Council (BBSRC) and the European Union (training network HPRN-CT-2002-00262: BioInteractions and FP6-PHARMA-PLANTA consortium). We thank D.G. Robinson (University of Heidelberg, Germany) for the generous gift of the rabbit polyclonal antiserum raised against the cytosolic domain of SYP21. We also thank Chris Hawes (Oxford Brookes University, Oxford, UK) for the generous gift of transgenic tobacco plants producing the Golgi marker ST-GFP and Nathalie Leborgne-Castel (University of Dijon, France) for transgenic

tobacco plants expressing Bob-TIP-26-1-GFP. O.F. thanks the BBSRC for the QUOTA studentship to support university fees and the European Union for the personal allowance for maintenance. L.L.P.d. thanks CAPES-Brasil for a PhD studentship. We also thank Gareth Howell (University of Leeds, UK) for help with the Biolmaging facility and Federica Brandizzi (University of Saskatoon, Canada) for scientific discussion and advice with the tobacco leaf infiltration method.

Received December 11, 2005; revised June 29, 2006; accepted July 19, 2006; published August 25, 2006.

REFERENCES

- Bassham, D.C., Gal, S., da Silva Conceicao, A., and Raikhel, N.V.** (1995). An Arabidopsis syntaxin homologue isolated by functional complementation of a yeast pep12 mutant. *Proc. Natl. Acad. Sci. USA* **92**, 7262–7266.
- Bassham, D.C., and Raikhel, N.V.** (1999). The pre-vacuolar t-SNARE AtPEP12p forms a 20S complex that dissociates in the presence of ATP. *Plant J.* **19**, 599–603.
- Bassham, D.C., Sanderfoot, A.A., Kovaleva, V., Zheng, H., and Raikhel, N.V.** (2000). AtVPS45 complex formation at the trans-Golgi network. *Mol. Biol. Cell* **11**, 2251–2265.
- Becherer, K.A., Rieder, S.E., Emr, S.D., and Jones, E.W.** (1996). Novel syntaxin homologue, Pep12p, required for the sorting of luminal hydrolases to the lysosome-like vacuole in yeast. *Mol. Biol. Cell* **7**, 579–594.
- Bonifacino, J.S., and Glick, B.S.** (2004). The mechanisms of vesicle budding and fusion. *Cell* **116**, 153–166.
- Borgese, N., Colombo, S., and Pedrazzini, E.** (2003). The tale of tail-anchored proteins: Coming from the cytosol and looking for a membrane. *J. Cell Biol.* **161**, 1013–1019.
- Brandizzi, F., Hanton, S., DaSilva, L.L., Boevink, P., Evans, D., Oparka, K., Denecke, J., and Hawes, C.** (2003). ER quality control can lead to retrograde transport from the ER lumen to the cytosol and the nucleoplasm in plants. *Plant J.* **34**, 269–281.
- Casadaban, M.J., and Cohen, S.N.** (1980). Analysis of gene control signals by DNA fusion and cloning in *Escherichia coli*. *J. Mol. Biol.* **138**, 179–207.
- Chatre, L., Brandizzi, F., Hocquellet, A., Hawes, C., and Moreau, P.** (2005). Sec22 and Memb11 are v-SNAREs of the anterograde endoplasmic reticulum-Golgi pathway in tobacco leaf epidermal cells. *Plant Physiol.* **139**, 1244–1254.
- Chen, Y.A., and Scheller, R.H.** (2001). SNARE-mediated membrane fusion. *Nat. Rev. Mol. Cell Biol.* **2**, 98–106.
- Crofts, A.J., Leborgne-Castel, N., Hillmer, S., Robinson, D.G., Phillipson, B., Carlsson, L.E., Ashford, D.A., and Denecke, J.** (1999). Saturation of the endoplasmic reticulum retention machinery reveals anterograde bulk flow. *Plant Cell* **11**, 2233–2247.
- Darsow, T., Rieder, S.E., and Emr, S.D.** (1997). A multispecificity syntaxin homologue, Vam3p, essential for autophagic and biosynthetic protein transport to the vacuole. *J. Cell Biol.* **138**, 517–529.
- daSilva, L.L., Foresti, O., and Denecke, J.** (2006). Targeting of the plant vacuolar sorting receptor BP80 is dependent on multiple sorting signals in the cytosolic tail. *Plant Cell* **18**, 1477–1497.
- daSilva, L.L., Taylor, J.P., Hadlington, J.L., Hanton, S.L., Snowden, C.J., Fox, S.J., Foresti, O., Brandizzi, F., and Denecke, J.** (2005). Receptor salvage from the prevacuolar compartment is essential for efficient vacuolar protein targeting. *Plant Cell* **17**, 132–148.
- da Silva Conceicao, A., Marty-Mazars, D., Bassham, D.C., Sanderfoot, A.A., Marty, F., and Raikhel, N.V.** (1997). The syntaxin homologue AtPEP12p resides on a late post-Golgi compartment in plants. *Plant Cell* **9**, 571–582.
- Fasshauer, D.** (2003). Structural insights into the SNARE mechanism. *Biochim. Biophys. Acta* **1641**, 87–97.
- Geelen, D., Leyman, B., Batoko, H., Di Sansebastiano, G.P., Moore, I., and Blatt, M.R.** (2002). The abscisic acid-related SNARE homologue NtSyr1 contributes to secretion and growth: Evidence from competition with its cytosolic domain. *Plant Cell* **14**, 387–406.
- Gerrard, S.R., Levi, B.P., and Stevens, T.H.** (2000a). Pep12p is a multifunctional yeast syntaxin that controls entry of biosynthetic, endocytic and retrograde traffic into the prevacuolar compartment. *Traffic* **1**, 259–269.
- Gerrard, S.R., Mecklem, A.B., and Stevens, T.H.** (2000b). The yeast endosomal t-SNARE, Pep12p, functions in the absence of its trans-membrane domain. *Traffic* **1**, 45–55.
- Gillingham, A.K., and Munro, S.** (2003). Long coiled-coil proteins and membrane traffic. *Biochim. Biophys. Acta* **1641**, 71–85.
- Hardwick, K.G., Boothroyd, J.C., Rudner, A.D., and Pelham, H.R.** (1992). Genes that allow yeast cells to grow in the absence of the HDEL receptor. *EMBO J.* **11**, 4187–4195.
- Harsay, E., and Schekman, R.** (2002). A subset of yeast vacuolar protein sorting mutants is blocked in one branch of the exocytic pathway. *J. Cell Biol.* **156**, 271–285.
- Hong, W.** (2005). SNAREs and traffic. *Biochim. Biophys. Acta* **1744**, 493–517.
- Jahn, R., Lang, T., and Sudhof, T.C.** (2003). Membrane fusion. *Cell* **112**, 519–533.
- Jurgens, G.** (2004). Membrane trafficking in plants. *Annu. Rev. Cell Dev. Biol.* **20**, 481–504.
- Li, Y.B., Rogers, S.W., Tse, Y.C., Lo, S.W., Sun, S.S., Jauh, G.Y., and Jiang, L.** (2002). BP-80 and homologs are concentrated on post-Golgi, probable lytic prevacuolar compartments. *Plant Cell Physiol.* **43**, 726–742.
- Maliga, P., Sz-Breznovits, A., and Marton, L.** (1973). Streptomycin-resistant plants from callus culture of haploid tobacco. *Nat. New Biol.* **244**, 29–30.
- Mitsuhashi, N., Shimada, T., Mano, S., Nishimura, M., and Hara-Nishimura, I.** (2000). Characterization of organelles in the vacuolar-sorting pathway by visualization with GFP in tobacco BY-2 cells. *Plant Cell Physiol.* **41**, 993–1001.
- Murashige, R., and Skoog, F.** (1962). A revised medium for rapid growth and bioassays with tobacco tissue cultures. *Physiol. Plant.* **15**, 473–497.
- Nebenfuhr, A.** (2002). Vesicle traffic in the endomembrane system: A tale of COPs, Rabs and SNAREs. *Curr. Opin. Plant Biol.* **5**, 507–512.
- Neuhaus, J.-M., and Boevink, P.** (2001). The green fluorescent protein (GFP) as a reporter in plant cells. In *Plant Cell Biology*, C. Hawes and B. Satiat-Jeunemaitre, eds (Oxford, UK: Oxford University Press), pp. 127–142.
- Niihama, M., Uemura, T., Saito, C., Nakano, A., Sato, M.H., Tasaka, M., and Morita, M.T.** (2005). Conversion of functional specificity in Qb-SNARE VT11 homologues of Arabidopsis. *Curr. Biol.* **15**, 555–560.
- Oliviusson, P., Heinzerling, O., Hillmer, S., Hinz, G., Tse, Y.C., Jiang, L., and Robinson, D.G.** (2006). Plant retromer, localized to the prevacuolar compartment and microvesicles in Arabidopsis, may interact with vacuolar sorting receptors. *Plant Cell* **18**, 1239–1252.
- Paris, N., and Neuhaus, J.M.** (2002). BP-80 as a vacuolar sorting receptor. *Plant Mol. Biol.* **50**, 903–914.
- Pfeffer, S.R.** (1999). Transport-vesicle targeting: Tethers before SNAREs. *Nat. Cell Biol.* **1**, E17–E22.
- Phillipson, B.A., Pimpl, P., daSilva, L.L., Crofts, A.J., Taylor, J.P., Movafeghi, A., Robinson, D.G., and Denecke, J.** (2001). Secretory bulk flow of soluble proteins is COPII dependent. *Plant Cell* **13**, 2005–2020.

- Pimpl, P., Hanton, S.L., Taylor, J.P., Pinto-DaSilva, L.L., and Denecke, J.** (2003). The GTPase ARF1p controls the sequence-specific vacuolar sorting route to the lytic vacuole. *Plant Cell* **15**, 1242–1256.
- Pimpl, P., Taylor, J.P., Snowden, C.J., Hillmer, S., Robinson, D.G., and Denecke, J.** (2006). Golgi-mediated vacuolar sorting of the ER chaperone BiP may play an active role in quality control within the secretory pathway. *Plant Cell* **18**, 198–211.
- Pratelli, R., Sutter, J.U., and Blatt, M.R.** (2004). A new catch in the SNARE. *Trends Plant Sci.* **9**, 187–195.
- Reisen, D., Marty, F., and Leborgne-Castel, N.** (2005). New insights into the tonoplast architecture of plant vacuoles and vacuolar dynamics during osmotic stress. *BMC Plant Biol.* **5**, 13.
- Saito, C., Ueda, T., Abe, H., Wada, Y., Kuroiwa, T., Hisada, A., Furuya, M., and Nakano, A.** (2002). A complex and mobile structure forms a distinct subregion within the continuous vacuolar membrane in young cotyledons of Arabidopsis. *Plant J.* **29**, 245–255.
- Sanderfoot, A.A., Ahmed, S.U., Marty-Mazars, D., Rapoport, I., Kirchhausen, T., Marty, F., and Raikhel, N.V.** (1998). A putative vacuolar cargo receptor partially colocalizes with AtPEP12p on a prevacuolar compartment in Arabidopsis roots. *Proc. Natl. Acad. Sci. USA* **95**, 9920–9925.
- Sanderfoot, A.A., Assaad, F.F., and Raikhel, N.V.** (2000). The Arabidopsis genome. An abundance of soluble N-ethylmaleimide-sensitive factor adaptor protein receptors. *Plant Physiol.* **124**, 1558–1569.
- Sanderfoot, A.A., Kovaleva, V., Bassham, D.C., and Raikhel, N.V.** (2001a). Interactions between syntaxins identify at least five SNARE complexes within the Golgi/prevacuolar system of the Arabidopsis cell. *Mol. Biol. Cell* **12**, 3733–3743.
- Sanderfoot, A.A., Kovaleva, V., Zheng, H., and Raikhel, N.V.** (1999). The t-SNARE AtVAM3p resides on the prevacuolar compartment in Arabidopsis root cells. *Plant Physiol.* **121**, 929–938.
- Sanderfoot, A.A., Pilgrim, M., Adam, L., and Raikhel, N.V.** (2001b). Disruption of individual members of Arabidopsis syntaxin gene families indicates each has essential functions. *Plant Cell* **13**, 659–666.
- Sanderfoot, A.A., and Raikhel, N.V.** (1999). The specificity of vesicle trafficking: Coat proteins and SNAREs. *Plant Cell* **11**, 629–641.
- Sato, M.H., Nakamura, N., Ohsumi, Y., Kouchi, H., Kondo, M., Hara-Nishimura, I., Nishimura, M., and Wada, Y.** (1997). The AtVAM3 encodes a syntaxin-related molecule implicated in the vacuolar assembly in *Arabidopsis thaliana*. *J. Biol. Chem.* **272**, 24530–24535.
- Seaman, M.N.** (2005). Recycle your receptors with retromer. *Trends Cell Biol.* **15**, 68–75.
- Seaman, M.N., Marcusson, E.G., Cereghino, J.L., and Emr, S.D.** (1997). Endosome to Golgi retrieval of the vacuolar protein sorting receptor, Vps10p, requires the function of the VPS29, VPS30, and VPS35 gene products. *J. Cell Biol.* **137**, 79–92.
- Seaman, M.N., McCaffery, J.M., and Emr, S.D.** (1998). A membrane coat complex essential for endosome-to-Golgi retrograde transport in yeast. *J. Cell Biol.* **142**, 665–681.
- Sohn, E.J., Kim, E.S., Zhao, M., Kim, S.J., Kim, H., Kim, Y.W., Lee, Y.J., Hillmer, S., Sohn, U., Jiang, L., and Hwang, I.** (2003). Rha1, an Arabidopsis Rab5 homolog, plays a critical role in the vacuolar trafficking of soluble cargo proteins. *Plant Cell* **15**, 1057–1070.
- Surpin, M., Zheng, H., Morita, M.T., Saito, C., Avila, E., Blakeslee, J.J., Bandyopadhyay, A., Kovaleva, V., Carter, D., Murphy, A., Tasaka, M., and Raikhel, N.** (2003). The VTI family of SNARE proteins is necessary for plant viability and mediates different protein transport pathways. *Plant Cell* **15**, 2885–2899.
- Tse, Y.C., Mo, B., Hillmer, S., Zhao, M., Lo, S.W., Robinson, D.G., and Jiang, L.** (2004). Identification of multivesicular bodies as prevacuolar compartments in *Nicotiana tabacum* BY-2 cells. *Plant Cell* **16**, 672–693.
- Ueda, T., Uemura, T., Sato, M.H., and Nakano, A.** (2004). Functional differentiation of endosomes in Arabidopsis cells. *Plant J.* **40**, 783–789.
- Uemura, T., Ueda, T., Ohniwa, R.L., Nakano, A., Takeyasu, K., and Sato, M.H.** (2004). Systematic analysis of SNARE molecules in Arabidopsis: Dissection of the post-Golgi network in plant cells. *Cell Struct. Funct.* **29**, 49–65.
- Uemura, T., Yoshimura, S.H., Takeyasu, K., and Sato, M.H.** (2002). Vacuolar membrane dynamics revealed by GFP-AtVam3 fusion protein. *Genes Cells* **7**, 743–753.
- Varlamov, O., Volchuk, A., Rahimian, V., Doege, C.A., Paumet, F., Eng, W.S., Arango, N., Parlati, F., Ravazzola, M., Orci, L., Sollner, T.H., and Rothman, J.E.** (2004). i-SNAREs: Inhibitory SNAREs that fine-tune the specificity of membrane fusion. *J. Cell Biol.* **164**, 79–88.
- Wada, Y., Nakamura, N., Ohsumi, Y., and Hirata, A.** (1997). Vam3p, a new member of syntaxin related protein, is required for vacuolar assembly in the yeast *Saccharomyces cerevisiae*. *J. Cell Sci.* **110**, 1299–1306.
- Wada, Y., Ohsumi, Y., and Anraku, Y.** (1992). Genes for directing vacuolar morphogenesis in *Saccharomyces cerevisiae*. I. Isolation and characterization of two classes of vam mutants. *J. Biol. Chem.* **267**, 18665–18670.
- Wooding, S., and Pelham, H.R.** (1998). The dynamics of golgi protein traffic visualized in living yeast cells. *Mol. Biol. Cell* **9**, 2667–2680.
- Yano, D., Sato, M., Saito, C., Sato, M.H., Morita, M.T., and Tasaka, M.** (2003). A SNARE complex containing SGR3/AtVAM3 and ZIG/VTI11 in gravity-sensing cells is important for Arabidopsis shoot gravitropism. *Proc. Natl. Acad. Sci. USA* **100**, 8589–8594.
- Zerial, M., and McBride, H.** (2001). Rab proteins as membrane organizers. *Nat. Rev. Mol. Cell Biol.* **2**, 107–117.
- Zheng, H., von Mollard, G.F., Kovaleva, V., Stevens, T.H., and Raikhel, N.V.** (1999). The plant vesicle-associated SNARE AtVTI1a likely mediates vesicle transport from the trans-Golgi network to the prevacuolar compartment. *Mol. Biol. Cell* **10**, 2251–2264.